COORDINATED NAVIGATION OF SPHERICAL ROBOTS IN THREE-DIMENSIONAL WORKSPACE: INDEPENDENT AND ORDER CONSTRAINED SCENARIOS

by

Barış ULUTAŞ

B.S. in Electrical & Electronics Engineering, Boğaziçi University, 2005

Submitted to the Institute for Graduate Studies in
Science and Engineering in partial fulfillment of
the requirements for the degree of
Master of Science

Graduate Program in Electrical & Electronics Engineering
Boğaziçi University

2008

ACKNOWLEDGEMENTS

I would like to express my sincere thanks to my advisor Prof. Işıl Bozma and my committee member Prof. Türkan Haliloğlu, not only for their guiding and encouragement, but also for their patience throughout the preparation of this thesis.

I am grateful to Assist. Prof. Mehmet Akar for his kind attitude.

I would like to thank TUBITAK for an academic scholarship grant during my master education.

Last but not least, I would like to express my gratitude to my friends and my family for their invaluable support in my whole life.

ABSTRACT

COORDINATED NAVIGATION OF SPHERICAL ROBOTS IN THREE-DIMENSIONAL WORKSPACE: INDEPENDENT AND ORDER CONSTRAINED SCENARIOS

In this thesis, the coordinated navigation of multiple disk-shaped robots is extended to three-dimensional workspace. The robots are assumed all to be spherical and residing within the same spherical workspace. In addition, each robot has a sensory range which determines its knowledge of the workspace. The robots task is to navigate from an arbitrary initial location to a final goal position. Two different scenarios are considered: independent navigation and order constrained navigation. In the independent case, all the robots are physically independent from each other. In order constrained navigation, we consider the case where the robots are ordered and the distance between adjacent robots is required to remain fixed throughout the motion by the help of imaginary links. It is shown that both types of motion can be achieved by using feedback-based strategies using artificial potential functions. The artificial potential functions is based on the extension and adaptation of a construction formerly proposed and proven for the two-dimensional case. Extensive simulations serve to demonstrate the performance of the approach under varying difficulty of tasks and noises. In addition, the theory developed in order constrained navigation is utilized to investigate protein folding kinetics. Results obtained from simulations are validated by the known experimental results.

ÖZET

KÜRESEL ROBOTLARIN EŞGÜDÜMLÜ GEZİNİMİ: BAĞIMSIZ VE SIRA KISITLAMALI SENARYOLAR

Bu tezde, çoklu disk şekilli robotların eşgüdümlü gezinimi üç boyutlu çalışma alanına genişletilmiştir. Robotların küresel oldukları ve aynı çalışma alanında bulundukları varsayılmıştır. Ayrıca, her robotun çalışma alanı bilgisini belirleyen bir duyumsal alanı vardır. Robotların görevi rastsal bir başlangıç konumundan bir son konuma ulaşmaktır. İki farklı senaryo dikkate alınmıştır: bağımsız gezinim ve sıra kısıtlamalı gezinim. Bağımsız gezinimde, tüm robotlar fiziksel olarak birbirlerinden bağımsızdır. Kısıtlı senaryoda, tüm robotların sıralı olduğu ve komşu robotlar arasındaki mesafenin gezinim süresince sabit kaldığı durum dikkate alınmıştır. İki tür harekette yapay potensiyel işlev kullanılarak elde edilen geri beslemeli strateji kullanılarak kotarılabilir. Yapay potensiyel işlevler daha önce iki boyutlu durum için önerilen ve ispatlanan yapay potensiyel işlevin genişletilmesi ve uyarlanması ile elde edilmiştir. Kapsamlı benzeşimler yaklaşımın farklı görev zorluğu ve gürültü değerlerindeki başarımını göstermeye yardımcı olur. Ayrıca, sıra kısıtlamalı gezinimde geliştirilen kuramdan protein katlanma devinimi incelemek için yararlanılmıştır. Benzetimlerden elde edilen sonuçlar, deneysel sonuçlarla tasdik edilmiştir.

TABLE OF CONTENTS

LIST OF FIGURES

LIST OF TABLES

LIST OF SYMBOLS/ABBREVIATIONS

$\|.\|$	Norm of a vector
$a_i \in Z^+$	Cardinality of A_i
A_i	Index set of adjacent robot pairs
$b \in R^{3p}$	Aggregate vector of all robots' positions
$b_i \in R^3$	Position vector of robot i with respect to world frame
${}^{B_2}b_i \in R^3$	Position vector of robot i with respect to B_2 frame
B_i	Robot frame centered on robot $i-1$
$c_i \in R^{3p_i}$	Aggregate vector of all robots' positions in P_i
$c_{g_i} \in R^{3p_i}$	Aggregate vector of all robots' goal positions in P_i
$d_{mj} \in R^3$	Distance vector of robots m and j
$D_{b_i}\varphi_i$	Gradient of φ_i with respect to b_i
$e_i \in R^p$	Unit base vector in R^p
F_i	Free configuration space known by robot i
$g \in R^{3p}$	Aggregate vector of all robots' goal positions
$g_i \in R^3$	Goal vector of robot i
K_i	Index set of robots that i^{th} robot can get data in order constrained navigation
$k_i \in Z^+$	Cardinality of K_i
M_i	Set of order numbers of robots that i^{th} robot can sense
$l_i \in Z^+$	Lowest order number in M_i
$o_i \in Z^+$	Order number of robot i in P
I_i	i^{th} robot's position with respect to B_i frame
$J \in R^{3\times3}$	Rotation matrix
$p \in Z^+$	Number of the robots in set P
P	Index set of all robots
P_i	Index set of robots that i^{th} robot can sense
T_i	i^{th} transform matrix
Q_i	Index set of robot pairs in P_i
Q_{i_0}	Index set of robot pairs in P_i including workspace boundary

$u_i \in Z^+$	Highest order number in M_i
s	State vector in order constrained navigation
$s_i \in R^{3k_i}$	Aggregate vector of positions of robots in K_i
$w_i \in SO(2k_i - 5)$	Aggregate torsion angle vector of i^{th} robot
$w_{gi} \in SO(2k_i - 5)$	Aggregate goal torsion angle vector of i^{th} robot
X	Index set of θ angles
Y	Index set of ϕ angles
Z_i	Index set of robot pairs in K_i
$z_i \in Z^+$	Cardinality of Z_i
β_i	Repulsive part of the artificial potential function of i^{th} robot
γ_i	Attractive part of the artificial potential function of i^{th} robot
$\delta_{mj} \in R^+$	Pairwise relative distance of robots m and j
$\Theta \in SO(p-2)$	Aggregate vector of all θ angles
$\Theta_i \in SO(k_i - 2)$	Aggregate vector of θ angles that i^{th} robot uses
κ	Aggregate extrinsic position angles
$\lambda \in R^+$	Distance between adjacent robot pairs in order constrained navigation
$\mu_i \in R^+$	Sensory range of robot i
$\rho_{mj} \in R^+$	Sum of radiuses of robots m and j
$\rho_i \in R^+$	Radius of robot i
σ	Squashing function
σ_d	Sharpening function
$\Phi \in SO(p-3)$	Aggregate vector of all ϕ angles
$\Phi_i \in SO(k_i - 3)$	Aggregate vector of ϕ angles that i^{th} robot uses
φ_i	Artificial potential function for robot i in independent navigation
$\check{\varphi}_i$	Intrinsic artificial potential function for robot i in order constrained navigation
$\hat{\varphi}$	Extrinsic artificial potential function in order constrained navigation
APF	Artificial potential function

nal	Normalized angle length
nrc	Normalized robot collision
nrl	Normalized robot path length
PDB	Protein data bank
PRM	Probabilistic roadmaps
RRT	Rapidly-exploring random trees

1. Introduction

This thesis extends the geometrically simplified version of coordinated motion in 2D to three-dimensional (3D) workspace. There is a collection of 3D sphere-shaped robots in a 3D sphere-shaped workspace that can move simultaneously with others. Their task is to reach their pre-specified goal locations without any collisions along the way. From this perspective, each robot becomes a dynamic obstacle for the remaining robots. Two different scenarios are considered: independent and order constrained depending on whether each robot can move independently of each other or whether the robots are to be in a linear order with fixed distance constraints among any two consecutive pair. Furthermore, each robot has a specified sensory range and depending on the extent of this range, the information about other robots can vary from being complete to myopic. In the global case, the radius of communication is infinite and each robot is assumed to know the exact positions and sizes of all other robots. Depending on the extent of this radius, information gets more and more local and each robot has access to information of the robots which reside in its sensory range. Note that the extreme case corresponds to total blindness, where no communication is possible.

In the independent scenario, the coordinated navigation of multiple sphere-shaped robots in three-dimensional workspace is posed as a Nash game. The problem of robot navigation coordination sets the basis for a non-cooperative Nash game where each robot is an individual decision maker for its motion. In the order constrained scenario, each robot is viewed as being constrained by imaginary links to two neighboring robots with fixed distances between them which also prevails throughout their motion. As opposed to the classical robotic manipulator problems where only the end-effector is of concern, the complete robot structure starts from an initial position in 3-D and needs to navigate to a final goal position without any collisions along the way. A two level approach is proposed. At the lower level, the robot structure is made to conform to the goal structure using artificial potential functions based on torsion angles without any consideration for alignment in 3D space. Depending on the sensory radius, complete to myopic information regarding other robots may be available to each robot. At the

higher level, the complete structure is made to align with the goal position using simple attractive potentials.

1.1. Related Literature

The literature survey covers the two cases seperately. First, a survey on independent navigation is presented. Following, we report on work related to order constrained navigation.

1.1.1. Independent Navigation

In the literature, work on multi-robot navigation is classified into two main categories: computational geometry based and reactive approaches.

In the computational geometry based approaches, the kinematic planning is separated from the dynamic control stage. In general, they are based on advanced search techniques in the configuration space[8]. The PRMs(Probabilistic Roadmaps)[9] and RRTs(Rapidly-exploring Random Trees)[10] are the most prominent of these approaches. Planning is achieved in general either in a centralized or decoupled manner [39, 36, 40]. An approach that integrates the two is proposed in probabilistic roadmaps – where simple roadmaps are combined together into composite roadmaps [44]. In cases where each robot's path is completely known a priori and can be decomposed into segments whose collision properties are known, pairwise robot collision constraints is formulated as a mixed integer nonlinear program with global convergence properties [45].

Alternatively, there has been a growing trend in using reactive approaches in multi-robot scenarios. [38, 35]. Heuristic reactive behaviors that implement various formations in multirobot teams are demonstrated on unmanned ground vehicles in [42]. Various forms of artificial potential functions have been constructed – with the aim of establishing a formal analysis framework while being simple[41], [28], [29],[30],[31] ,[32]. In general, the major shortcoming of this approach has been the difficulty of analytic

tractability [37]. The main drawback of the artificial potential based approaches is the local minima problem. In [23] a method which needs human interaction for escaping local minima proposed. The method has further been improved in [24] that has resulted in eliminating the human interaction. Although it can be applied to many degrees of freedom manipulators, it becomes intractable as the dimension increases further. In [25] and [21] the potential functions with local minima escape capabilities in high dimensional configuration spaces are presented. In [21] random walks are used to escape local minima. This method successfully applied to many practical problems [26], [51], [27]. An exact potential field planner for coordinated motion in disk-shaped worlds is presented in [33] – provided that at each instance, all robot positions are available and goal positions satisfy certain tightness restrictions. In this thesis, we generalize these results to three-dimensional workspace while considering the more realistic cases of both partial and noisy sensory information.

1.1.2. Order Constrained Navigation

Our survey on order constrained navigation has revealed that there is relatively less work reported on order constrained navigation. Two categories of work are considered to be related: highly articulated or redundant robots and robotic formations.

Order constrained navigation has similarities with the problem of motion planning of highly articulated or redundant chains [1], [2]. A redundant manipulator has more degrees of freedom than it needs to execute the given job. Redundancy is important for challenging tasks like rescuing in complex environments such as space exploration. The practical examples of the hyper redundant robots are investigated in [3],[4], [5], [6] and [7]. The motion planning of such systems is generally based on computational geometry based approaches. For example, RRTs are also easily applied to articulated bodies [11], [12], [13]. However as the dimension of the configuration space increases, the computational burden of the sampling based methods expands considerably. In order to decrease the computational burden, the biased sampling methods are begun to be considered [14],[15],[16],[17], [18],[19]. Morever, these methods are usually concerned with just the position of the end effector, order constrained navigation is concerned

with the navigation of whole structure from one configuration to another.

A second related line of work is the research in robotic formations and swarms. Here, again, the proposed approaches are based on either computational geometry or artificial potential functions. For example, multi-robot formation navigation is studied in [47]. A potential function is proposed for the case of moving targets and dynamic obstacles in [43] – where the problem of local minima is discussed. The problem of coordinated navigation while moving in formation is studied in [46], where a class of formation keeping control strategies are combined with a new dynamic window approach using navigation functions. In this thesis, artificial potential functions are applied to order constrained robots.

1.2. Contribution of the Thesis

The contributions of this thesis can be summarized as follows:

- The coordinated navigation of disk shaped robots generalized to 3-D by considering more realistic case of partial information of workspace.
- The performance of the independent navigation is tested against partial and noisy information.
- A novel method for navigation of highly articulated body like multi-robot team is introduced.
- The performance of order constrained navigation is tested against partial and noisy information.
- The applicability of theory developed in order constrained navigation to investigation of protein folding kinetics is proven by comparing the results obtain from simulation runs with the real experimental data.

1.3. Outline of the Thesis

The thesis is organized in the following chapters. The first chapter is an introduction to the thesis that presents related literature and a summary of the proposed

approaches. The generalization of the coordinated navigation of disk-shaped robots to 3-D with considering partial and noisy information is presented in Chapter 2. Chapter 3 presents a novel method for coordinated navigation of a sequence of sphere shaped robots that are ordered in a linear manner in three-dimensional workspace. In Chapter 4, applicability of the theory developed in order constrained navigation to protein folding kinetics investigation is tested.Results obtained from simulations are compared both with the experimental data and previous methods' data.

2. Independent Navigation

This chapter of the thesis extends the geometrically simplified version of coordinated motion to three-dimensional (3D) workspace. There is a collection of 3D sphere-shaped robots in a 3D sphere-shaped workspace that can move independently of and simultaneously with others. From this perspective, each robot becomes a dynamic obstacle for the remaining robots. Their task is reach their pre-specified goal locations without any collisions along the way. Furthermore, each robot has a specified sensory range and depending on the extent of this range, the information about other robots can vary from being complete to myopic. The problem formulation sets the basis for a semi-cooperative Nash game where each robot has an individual cost function and moves accordingly. This induces a differential game structure where the robots try to attain the Nash equilibrium point. The semi-cooperativity is attained by endowing with a cost function that not only encodes its goal position, but also those of robots within its sensory range while ensuring that there will be no collisions with these robots as well. This chapter of thesis investigates the generalization of these results to three-dimensional workspace with considering more realistic cases of both partial and noisy sensory information.

The organization of this chapter is as follows: Section 2.1 gives the problem statement. The notation is presented in Section 2.2. The game-theoretic formulation is presented in Section 2.3. In section 2.4, the simulation results are presented. Firstly, the performance metrics are defined. Following, statistical results from extensive simulations with perfect sensory information under varying communication ranges are discussed. At the end of the section, the robustness of the method against noise is tested with varying task difficulties.

2.1. Problem Statement

Consider a collection of p sphere-shaped robots – arbitrarily placed within a spherical workspace. We assume that:

- Each robot has ideal bounded torque actuators
- Each robot has perfect real time knowledge of its own position and target; and
- At each instant, each robot knows the sizes, the locations and the targets of only those robots within its sensory range,

The problem is to define a control strategy which ensures that all the robots move from their initial positions to their a priori specified target locations without any collisions along the way.

2.2. Notation

Each robot $i \in P = \{1, \ldots, p\}, p \in \mathbf{Z}^+$, is defined by its center point $b_i \in \mathbf{R^3}$, and its radius $\rho_i \in \mathbf{R^3}$ and has a specified goal position $g_i \in \mathbf{R^3}$ and a sensory radius $\mu_i \in \mathbf{R}$. It can communicate with only robots $P_i = \{1, \ldots, p_i\}, p_i \in \mathbf{Z}^+$ that are within this range. The state vector of robots' instant and goal positions in P_i, $c_i \in \mathbf{R^{3p_i}}$ and $c_{g_i} \in \mathbf{R^{3p_i}}$ is defined as $c_i = \sum_{j \in P_i} b_j \otimes e_j$ and $c_{g_i} = \sum_{j \in P_i} g_j \otimes e_j$ respectively, where $e_1, e_2, \ldots, e_{p_i} \in \mathbf{R^{p_i}}$ are the unit base vectors in $\mathbf{R^{p_i}}$. Identically, the state vector of all robots' instant and goal positions, $b \in \mathbf{R^{3p}}$ and $g \in \mathbf{R^{3p}}$ is defined as $b = \sum_{j \in P} b_j \otimes e_j$ and $g = \sum_{j \in P} g_j \otimes e_j$, respectively.

The index set of robot pairs in P_i is defined by $Q_i = \{(m, j) | m, j \in P_i, m < j\}$. The distance d_{mj} for robot pairs $(m, j) \in Q_i$ is defined as $d_{mj} = b_m - b_j$.The robots' pairwise relative distance is $\delta_{mj} = \| d_{mj} \|$. The index set of robot pairs in P_i including the workspace boundary as a zeroth sphere Q_{i_0} , is defined by $Q_{i_0} = Q_i \cup \{(0, j) | \forall j \in P_i\}$. Since robots cannot overlap each other, it is required that

$$\delta_{mj} \geq \rho_{mj} = \rho_m + \rho_j \qquad \forall (m, j) \in Q_i \tag{2.1}$$

In order to locate each robot in workspace that is bounded by an outer sphere of radius ρ_0, it is also required that

$$\| b_j \| \leq \rho_{0j} = \rho_0 - \rho_j \qquad \forall j \in P_i \tag{2.2}$$

The *free robot configuration space* F_i known by i^{th} robot is defined as the subset of robot positions in $\mathbf{R^{3p_i}}$ which satisfy (2.1) and (2.2).

$$F_i = \{c_i \in \mathbf{R^{3p_i}} | (\forall j \in P_i, \parallel b_j \parallel \leq \rho_{0j}) \\ \wedge (\forall (m,j) \in Q_i, \delta_{mj} \geq \rho_{mj})\} \tag{2.3}$$

2.3. Game-Theoretic Framework

The problem is formulated as a semi-cooperative Nash game. First of all,

- Each robot $i \in P$ has a cost function $\varphi_i : F_i \rightarrow [0,1]$,
- The terms of the cost φ_i change as the set P_i changes,
- At each instant, each robot moves as to minimize its cost function,

The Nash equilibrium $b^* \in \mathbf{R^{3p}}$ is defined as $b^* = \left[b_1^*, \ldots, b_p^*\right]$ where

$$b_i^* \in \arg\min_{b_i} \varphi_i(b_1^*, \ldots, b_{i-1}^*, b_i, b_{i+1}^*, \ldots, b_p^*) \tag{2.4}$$

2.3.1. Cost Functions

The cost function $\varphi_i : F_i \rightarrow [0,1]$ of each i^{th} robot is constructed following the method presented in [33]:

$$\varphi_i = \sigma_d \circ \sigma \circ \widehat{\varphi}_i(c_i) \tag{2.5}$$

It encodes its own goal location and, the sizes and present states of the robots (including its own) that are within its sensory range. The function $\widehat{\varphi}_i : F_i \rightarrow [0,\infty)$ uses two functions $\gamma_i : F_i \rightarrow [0,\infty)$ and $\beta_i : F_i \rightarrow [0,\infty)$ in order to encode the goal point and

the obstacles of the robot:

$$\widehat{\varphi}_i(c_i) = \frac{(\gamma_i(c_i))^{n_i}}{\beta_i(c_i)} \quad n_i \in \mathbf{Z}^+ \tag{2.6}$$

While the distance from the goal is encoded by the numerator $\gamma_i(c_i) = (c_i - c_{g_i})^T(c_i - c_{g_i})$, the denominator encodes the distance from freespace boundary known by the robot and is defined as $\beta_i(c_i) = \prod_{\forall(m,j)\in Q_{i0}} \beta_{mj}(c_i)$, where $\forall(m,j) \in Q_i, \beta_{mj} = {\delta_{mj}}^2 - \rho_{mj}^2$ and $\forall j \in P_i, \beta_{0j} = {\rho_{0j}}^2 - \parallel b_j \parallel^2$. The freespace boundary known by the robot ∂F_i is the zero level set of ${\beta_i}^{-1}(0)$ and entails robots touching each other or the workspace boundary.

It is suggested to make the artificial potential function used both admissible and has a non-degenerate critical point at the goal point c_{g_i}. In order to make $\widehat{\varphi}_i$ admissible, we use a composition by $\sigma : [0,\infty) \to [0,1]$ which squashes $\widehat{\varphi}$, and defined by $\sigma = \frac{x}{x+1}$. Although $\sigma \circ \widehat{\varphi}$ function is admissible the goal point is still a degenerate critical point. To make goal point non-degenerate critical point, one more composition by the sharpening function $\sigma_d : [0,1] \to [0,1]$ is used. The function σ_d is defined by $\sigma_d(x) = x^{1/k}$. The resulting function of these two cascaded compositions can be denoted by φ_i which satisfies both suggestions.

Prop: The goal g is a Nash equilibrium point.

Proof: Note that $\varphi_i(b^*) = 0$ Since $\varphi_i \geq 0$ by definition, the result follows. □

2.4. Simulation Results

We now report on simulations associated with the construction in order to study the nature and the quality of the resulting navigation behavior. A Java-based simulator has been developed for this purpose. The complexity of the navigation task is defined

by the tightness of the goal position using a measure as presented in [33]:

$$tight = \frac{20000}{log_{10}(\prod_{(i,j)\in Q} \parallel g_i - g_j \parallel^2 - {\rho_{ij}}^2)} \tag{2.7}$$

It should be observed that the more packed the robots need to be at their goal locations, the bigger its value gets to be. The efficiency of the task accomplishment is measured by the normalized robot path length measure nrl as defined in [33]. This performance measure is the sum of all robots path lengths normalized by the sum of the Euclidean distance between initial and goal positions of the robots:

$$nrl = \frac{\sum_{i\in P} \int_0^{t_f} \parallel \dot{b}_i(t) \parallel dt}{\sum_{i\in P} \parallel b_i(0) - g_i \parallel} \tag{2.8}$$

Furthermore, the sensitivity of the system to imperfect sensory information is investigated. This is accomplished via subjecting all state readings to Gaussian noise with zero mean and given variance. If we denote the noise as η, the noisy robot position can be expressed as follows:

$$\tilde{b}_i = b_i + \eta \tag{2.9}$$

In this case, depending on the amount of noise, collisions among robots become possible. Letting N_C denote the number of collisions in a given simulation, the performance is measured using the normalized robot collision nrc defined as follows:

$$nrc = \frac{1000 * N_C}{\sum_{i\in P} \parallel b_i(0) - g_i \parallel} \tag{2.10}$$

Finally, all scenarios contain fifty robots. The goals are selected with five varying degrees of tightness – ranging from loose to close packedness as shown in Figure 2.2. For each goal configuration, 100 runs with random initial configurations are made. The

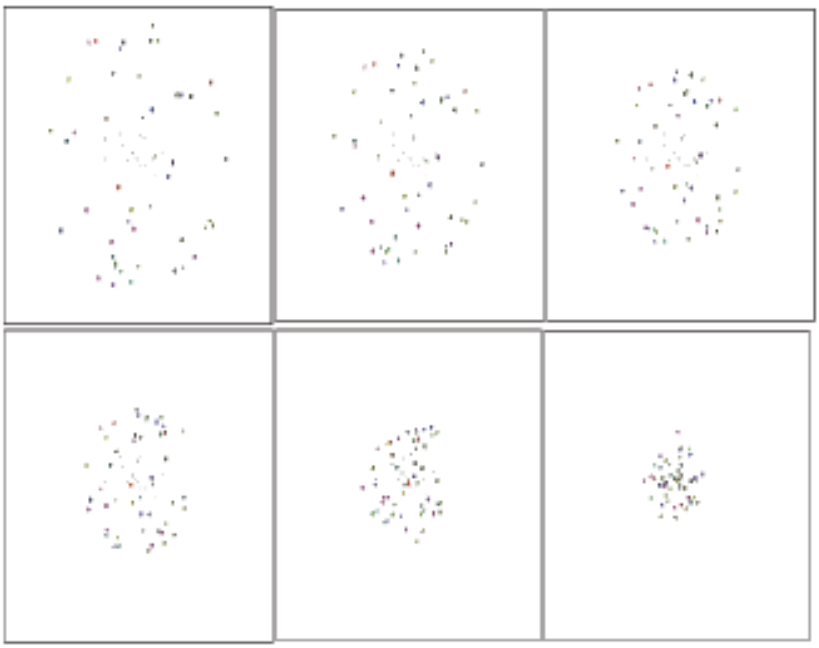

Figure 2.1. Snapshots from a simulation run of independent navigation

initial configurations are obtained by placing each robot randomly on surface of an outer sphere which includes all goal locations in its volume. The same initial configurations are used for all scenarios.

2.4.1. Complete & Perfect Sensory Case

In the first set of simulations, the robots are assumed to have complete and perfect sensory information. In Figure 2.3, the variation of the *nrl* with respect to tightness is presented. Interestingly, in contrast to its two-dimensional counterpart, the *nrl* and the corresponding standard deviation decrease as goal positions become more packed.

2.4.2. Complete & Noisy Sensory Case

Next, we consider the tightly packed goal configuration (of value 5.485). The robots continue to have complete sensory data, however sensory data is assumed to be noisy. For this purpose, five levels of noise is added to the robots positional readings: lowest (variance = 0.01), low (variance = 0.05), medium (variance = 0.10), high (variance = 0.15) and highest (variance = 0.20). For noise level, 100 runs with random

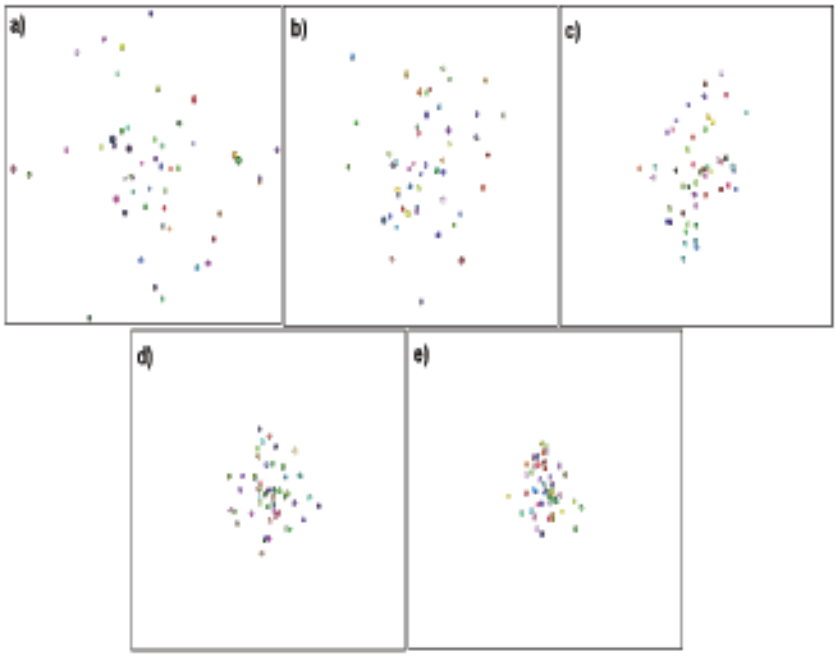

Figure 2.2. Task tightnesses of independent navigation. a) tight = 4,284 (relatively loose) , b) tight = 4,546 , c) tight = 4.999 , d) tight = 5,485 , e) tight = 6,028 (very pack)

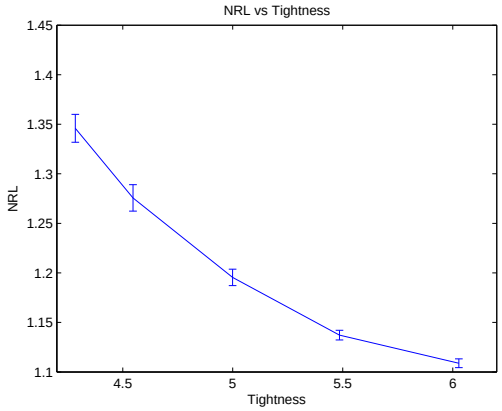

Figure 2.3. nrl vs tightness of complete and perfect sensory case in independent navigation.

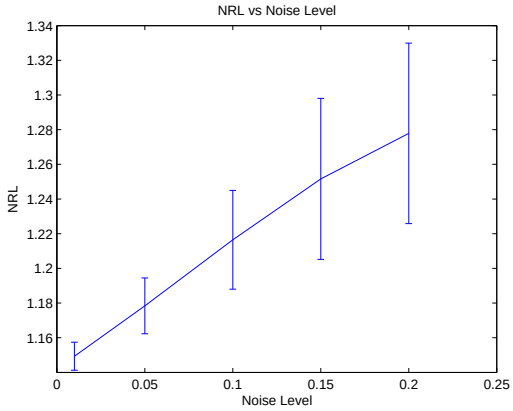

Figure 2.4. nrl vs noise level of complete and noisy sensory case in independent navigation.

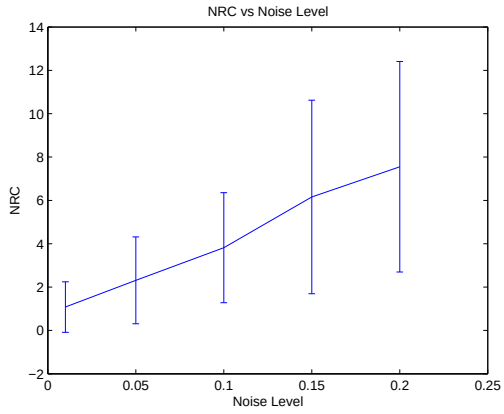

Figure 2.5. nrc vs noise level of complete and noisy sensory case in independent navigation.

initial configurations are simulated.

Figure 2.4 shows that as noise increases, so does *nrl* value. It can be said that as the noise level increases, the probability of the misguidance also increases.

Figure 2.5 reveals a positive correlation between noise level and *nrc*. The higher the sensor inaccuracy, the higher the *nrc* value. However, it should also be noted that although the increase in noise level increases *nrc* value, its value does not seem to grow exponentially. Rather it is observed to stay within a certain level. It can be said that as noise level increases the probability of collision among robots increases.

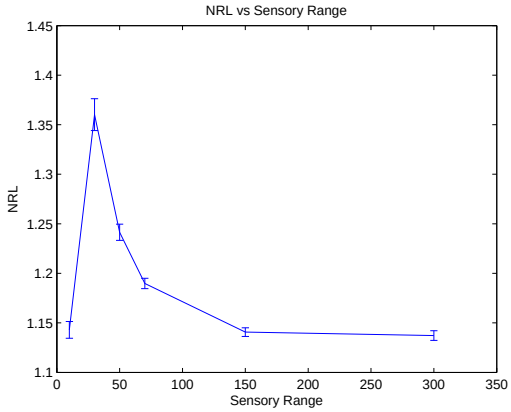

Figure 2.6. nrl vs sensory range of partial and perfect sensory case in independent navigation.

2.4.3. Partial & Perfect Sensory Case

Next, robot navigation behavior under partial, but perfect sensory data is investigated. Again, the tightly packed goal configuration (value 5.485) is taken. For this, each robot is assumed to have an identical sensory range in three directions $\mu_{c_i} = [n\rho_i, n\rho_i, n\rho_i]^T$. In these simulations, $n \in \{15, 45, 75, 105, 150, 450\}$ where it should be noted that small values indicate that each robot is able to pick up only very local information while as n value gets higher, each robot starts getting closer to having complete sensory data.

Figure 2.6 shows the change of nrl as a function of sensory range. As expected, if the robots are myopic, their nrl values tend to increase and as sensory range increases the nrl values decreases. The standard deviation also has an negative correlation with sensory range after a critical point.

2.4.4. Partial & Noisy Sensory Case

Next, robot navigation behaviour under partial, but noisy sensory data is investigated. Again, the tightly packed goal configuration (value 5.485) is taken. For this, again each robot is assumed to have an identical sensory range in three directions $\mu_i = [n\rho_i, n\rho_i, n\rho_i]^T$. In these simulations, $n \in \{15, 45, 75, 105, 150, 450\}$. The noise

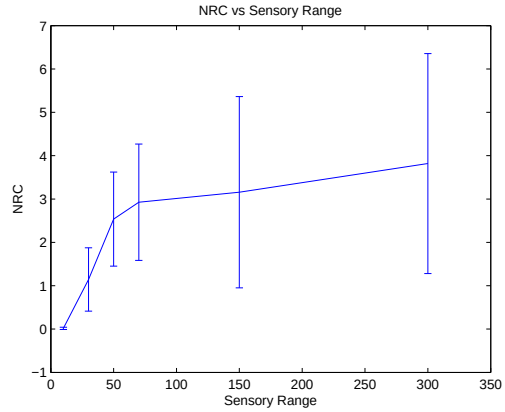

Figure 2.7. nrc vs sensory range of partial and noisy sensory case in independent navigation.

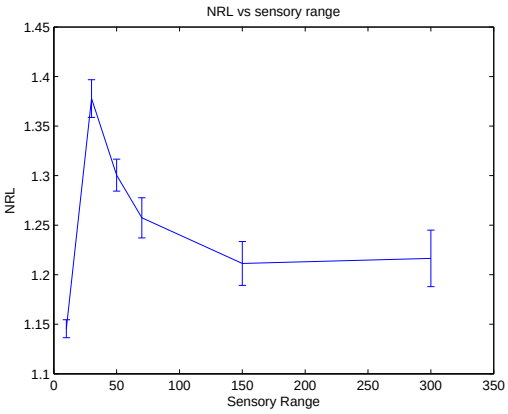

Figure 2.8. nrl vs sensory range of partial and noisy sensory case in independent navigation.

level is assumed to be of medium level. Figure 2.7 shows the *nrc* versus sensory range characteristics with noisy information. As the sensory range increases, the probability of the collisions also increases. As the sensory range increases, the probability of the misguidance increases. Figure 2.8 shows the *nrl* versus sensory range characteristics with noisy information. The graph is similar to the noise free information case.

3. Order Constrained Navigation

This chapter of the thesis addresses the coordinated navigation of a sequence of sphere shaped robots that are ordered in a linear manner in three-dimensional workspace. Such a scenario manifests itself in a variety of applications ranging from redundant manipulators to the modelling of protein folding dynamics in computational biology. In this setup, each robot can be viewed as being linked by imaginary links to two neighboring robots with fixed distances between them that prevails throughout its motion. As opposed to the classical robotic manipulator problems where only the end-effector is of concern, the complete robot structure has an initial conformation in 3-D and a final goal configuration which it needs to navigate to without any collisions among the robots along the course. Furthermore, each robot has a specified sensory range and depending on the extent of this range, the information about the other robots can vary from being complete to myopic. A two level approach is proposed: At the lower level, the intrinsic geometry of the goal configuration is attained using artificial potential functions based on torsion angles without any consideration for alignment in 3D space. Depending on the sensory radius, complete to myopic information regarding other robots may be available to each robot. At the higher level, the extrinsic geometry is attained via the alignment of the complete structure with the goal position using simple attractive potentials. Extensive simulations shows the performance of the suggested approach under varying difficulty and noise levels.

3.1. Problem Statement

Consider an ordered list of p spherical robots arranged in a chain-like structure in three-dimensional workspace where each robot – except those at the beginning or end of the chain – is linked to two neighboring robots by imaginary links. Furthermore, each robot has a specified sensory range. In case of perfect (noise free) information case, the following assumptions are made:

- Each robot has the ideal bounded torque actuators

- At any time, each robot can measure its own position exactly
- At any time, each robot has access to the positional information of all the robots whose sequence order is within the range as determined by the robots within its sensory range with the minimum and maximum order numbers.

The problem is then defined as having all the robots navigate to their goal positions in three-dimensional workspace without any collisions along the way.

3.2. Approach

3.2.1. Order Constrained Robots

Let us consider an ordered set of robots $P = \{1, \ldots, p\}, p \in \mathbf{Z}^+$ that are sequentially constrained together by imaginary links in three-dimensional (3-D) workspace. Suppose the distance between each adjacent pair is equal to $\lambda \in \mathbf{R}^+$. The configuration of the overall structure is defined in two levels based on intrinsic and extrinsic geometries. The intrinsic geometry refers to the relative positioning of the robots. It is defined by two state variables $\Theta \in \mathbf{SO(p-2)}$ and $\Phi \in \mathbf{SO(p-3)}$ that correspond to the torsion angles together define the intrinsic geometry of robots with respect to each other without any consideration to their placement in 3-D workspace. The index set of θ angles of a structure is defined as $X = \{1, \ldots, p-2\}$ and the index set of ϕ angles as $Y = \{2, \ldots, p-2\}$.The extrinsic geometry refers to the orientation and positioning of the robots in the three-dimensional workspace and is defined by two state variables $b_1 \in \mathbf{R^3}$ and $\kappa \in \mathbf{SO(3)}$ that define the location and orientation of the overall robot structure in 3-D workspace. Let's define the aggregate state space as $\mathbf{S} = \mathbf{SO(p-2)} \times \mathbf{SO(p-3)} \times \mathbf{R^3} \times \mathbf{SO(3)}$. Then altogether, these variables are concatenated to form the state vector $s \in \mathbf{S}$ where $s = \left[\Theta^T, \Phi^T, b_1^T, \kappa^T\right]^T$. The goal configuration in 3-D workspace is defined by $s_g \in \mathbf{S}$ where $s_g = \left[\Theta_g^T, \Phi_g^T, g_1^T, \kappa_g^T\right]^T$

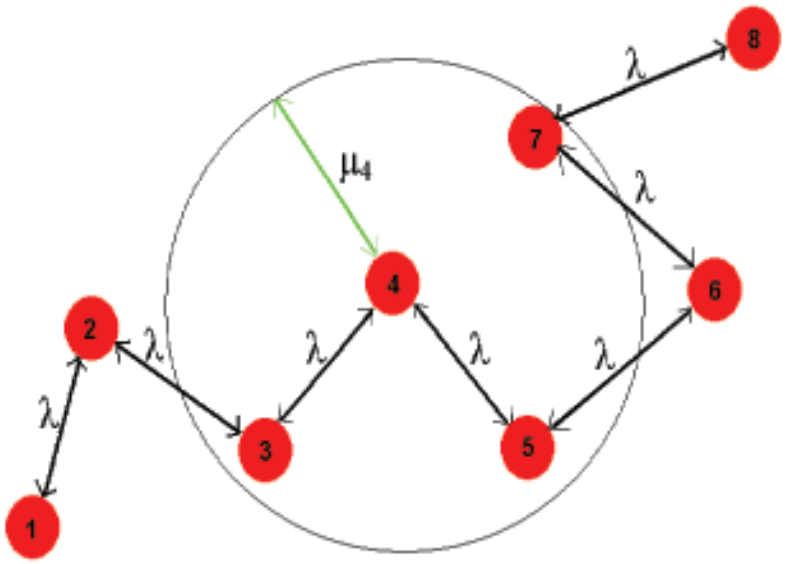

Figure 3.1. Set of robots that 4^{th} can get data is $K_4 = \{3(l_4), 4, 5, 6, 7(u_4)\}$

3.2.2. Each Robot as an Individual Player

Again like in independent scenario, each robot $i \in P$ has a radius $\rho_i \in \mathbf{R}$, a sensor range $\mu_i \in R$ and an order number in the sequence $o_i \in P$. In this scenario, i^{th} robot's location in 3-D workspace $b_i(s) \in \mathbf{R^3}$ is defined as a function of the state s. Similarly, its goal position $g_i(s_g) \in \mathbf{R^3}$ is also defined as a function of the goal s_g. The aggregate vector of instant positions of all robots $b(s) : \mathbf{S} \rightarrow \mathbf{R^{3p}}$ is defined as $b(s) = \sum_{i \in P} b_i(s) \bigotimes e_i$, where $e_1, e_2, \ldots, e_p \in \mathbf{R^p}$ are the unit base vectors in $\mathbf{R^p}$.

The visibility range of each robot i determines the state variables on which it has an effect. Let $M_i = \{o_j | j \in P, \parallel b_i(s) - b_j(s) \parallel < \mu_i\}$ denote the set of order numbers of robots that fall within its visibility range. Furthermore, let $l_i = \min M_i$ and $u_i = \max M_i$ respectively. It is assumed that each robot can get state data only from those robots whose orders lie in this range – namely $K_i = \{j | j \in P, l_i \leq o_j \leq u_i\}$. Define $k_i = |K_i|$ denote the cardinality of K_i. Each robot can see part of the state s defined by $\Theta_i \in \mathbf{SO(k_i - 2)}$ where $\Theta_i = [\theta_{l_i}, \cdots, \theta_{u_i - 2}]^T$ and $\Phi_i \in \mathbf{SO(k_i - 3)}$ where $\Phi_i = [\phi_{l_i + 1}, \cdots, \phi_{u_i - 2}]^T$. From its perspective, the overall constrained structure is defined by aggregate torsion angle vector $w_i \in \mathbf{SO(2k_i - 5)}$ where $w_i^T = [\Theta_i^T, \Phi_i^T]$.

The goal configuration is $w_{g_i}^T = [\Theta_{g_i}^T, \Phi_{g_i}^T]$. Let us define matrix $U_i \in \mathbf{R^{k_i \times k}}$, where

$$u_i[m,j] = \begin{cases} 1 & \text{if} \quad m = j \wedge m \in K_i \\ 0 & \text{otherwise} \end{cases} \tag{3.1}$$

Then, the aggregate positions of robots in K_i can be expressed by the function $s_i : \mathbf{S} \rightarrow \mathbf{R^{3k_i}}$ where $s_i(s) = U_i b(s)$.

The index set of robot pairs in K_i, $Z_i = \{(m,j)|m,j \in K_i, m < j\}$ has cardinality denoted by $z_i = |Z_i| = k_i(k_i-1)/2$. Similar to the independent scenario, for each robot pair $(m,j) \in Z_i$, letting d_{mj} denote $d_{mj}(s) = b_m(s) - b_j(s)$ and $\delta_{mj}(s) = \| d_{mj}(s) \|$. Let the index set of adjacent robot pairs denoted as $A_i = \{(m,j)|m,j \in K_i, m+1 = j\}$. The cardinality of A_i is denoted by $a_i = |A_i| = k_i - 1$. As the constraint length between adjacent robots is fixed to λ, the following holds:

$$\delta_{mj}(s) = \lambda \qquad \forall (m,j) \in A_i \tag{3.2}$$

3.2.3. 3-D Cartesian Coordinates from Torsion Angles

First, let us define a series of coordinate frames B_i, $\forall\, i \in P - \{1\}$, where each B_i denotes the frame centered on the robot of index $i-1$ such that its x axis is along the direction of the i^{th} robot and y axis is defined such that if $\frac{1}{2}\pi < \phi_{i-1} < \frac{3}{2}\pi$ then the $(i+1)^{th}$ robot is in the positive y coordinate. For B_2 since there is no ϕ_1 angle, we define y axis such that the second robot is in the positive y direction. Furthermore, let I_i denote position of the i^{th} ordered robot with respect to B_i. As the distance between two adjacent robots is λ,

$$I_i^T = \begin{bmatrix} \lambda & 0 & 0 \end{bmatrix} \tag{3.3}$$

The computation of the 3-D Cartesian coordinates is achieved in two steps: i)

First, the position of each robot is computed with respect to B_2 frame, ii) Next, B_2 frame is translated and rotated as to co-align with the world coordinate frame.

3.2.3.1. Cartesian Coordinates with respect to B_2 Frame. Given the state s, let ${}^{B_2}b_i(s)$ denote the position of the i^{th} robot with respect to the first frame B_2. This can be computed by defining a series of transformation matrices that recursively define the position of i^{th} robot with respect to B_2 frame. For $i > 1$, the i^{th} transformation matrix $T_i \in \mathbf{R^{3\times 3}}$ is defined as follows:

$$T_i = \begin{bmatrix} -\cos(\theta_i) & \sin(\theta_i) & 0 \\ -\sin(\theta_i)\cos(\phi_i) & -\cos(\theta_i)\cos(\phi_i) & -\sin(\phi_i) \\ -\sin(\theta_i)\sin(\phi_i) & -\cos(\theta_i)\sin(\phi_i) & \cos(\phi_i) \end{bmatrix} \text{ for } i > 1 \tag{3.4}$$

For $i = 1$, $T_1 \in \mathbf{R^{3\times 3}}$ is as follows:

$$T_1 = \begin{bmatrix} -\cos(\theta_1) & \sin(\theta_1) & 0 \\ \sin(\theta_1) & \cos(\theta_1) & 0 \\ 0 & 0 & -1 \end{bmatrix} \tag{3.5}$$

Then the position of the i^{th} robot with respect to B_2 frame can be expressed as;

$${}^{B_2}b_i(s) = \sum_{k=2}^{i}(\prod_{j=1}^{k-2} T_j I_k) \tag{3.6}$$

3.2.3.2. Aligning B_2 Frame with World Frame. In order to compute $b_i(s)$, B_2 frame is rotated and translated in order to align with the world frame as:

$$b_i(s) = J(\kappa)^{B_2}b_i(s) + b_1 \tag{3.7}$$

where $J(\kappa) \in R^3 \times R^3$ is the rotation matrix defined as

$$J(\kappa) = \begin{bmatrix} \cos\kappa_1 \cos\kappa_2 & -\sin\kappa_1 & \cos\kappa_1 \sin\kappa_2 \\ \sin\kappa_1 \cos\kappa_2 \cos\kappa_3 - \sin\kappa_2 \sin\kappa_3 & \cos\kappa_1 \cos\kappa_3 & \sin\kappa_1 \sin\kappa_2 \cos\kappa_3 - \cos\kappa_2 \sin\kappa_3 \\ \sin\kappa_1 \sin\kappa_3 \cos\kappa_2 + \sin\kappa_2 \cos\kappa_3 & \cos\kappa_1 \sin\kappa_3 & \sin\kappa_1 \sin\kappa_2 \sin\kappa_3 + \cos\kappa_2 \cos\kappa_3 \end{bmatrix} \tag{3.8}$$

3.2.3.3. Intrinsic and Extrinsic Geometry Configuration Spaces. The two-level nature of the approach induces separate, but related configuration spaces that are associated with intrinsic and extrinsic geometry. Furthermore, as each robot has its own visibility range, both vary as a function of K_i. Let G_i denote the intrinsic geometry configuration space as:

$$G_i = \{w_i \in \mathbf{SO(2k_i - 5)} | (\forall (m,j) \in Z_i, \|^{B_2} b_m(w_i) -^{B_2} b_j(w_i) \| \geq \rho_{mj}) \wedge (\forall (m,j) \in A_i, \|^{B_2} b_m(w_i) -^{B_2} b_j(w_i) \| = \lambda)\} \tag{3.9}$$

Let H_i denote the corresponding extrinsic geometry configuration space:

$$H_i = \left\{ s_i \in \mathbf{R^{3k_i}} | (\forall (m,j) \in Z_i, \delta_{mj} \geq \rho_{mj}) \wedge (\forall (m,j) \in A_i, \delta_{mj} = \lambda) \right\} \tag{3.10}$$

3.2.4. Artificial Potential Functions

The navigation of the robot team is achieved through a two-tier controller. For each robot, the control inputs coming from each tier are added together to generate the final control input. The lower tier is concerned with the collision free navigation of the robots in order to attain the intrinsic geometry of the goal configuration. Here, the control input is directly applied to the torsion angles. The construction of the controllers is based on artificial potential functions $\check{\varphi}_i : H_i \times G_i \rightarrow [0,1]$, $i \in P$, that

encode both the intrinsic geometry of the goal as well as collision-free configurations. As each robot has a limited visibility range, it is viewed as an individual player that sees only the part of the structure as designated by K_i and wants to have the associated torsion angles change accordingly. The control input to the associated state variables is then generated as the sum of individual contributions of individual robots as:

$$\begin{aligned} \dot{\theta}_i &= -\sum_{j=1}^{p} D_{\theta_i}\left(\check{\varphi}_j(s_j)\right) \\ \dot{\phi}_i &= -\sum_{j=1}^{p} D_{\phi_i}\left(\check{\varphi}_j(s_j)\right) \end{aligned}$$

The higher level is concerned with the translation and rotation of the overall structure in order to attain the extrinsic geometry. In this case, a simple attractive potential function $\hat{\varphi} : \mathbf{R^3} \times \mathbf{SO(3)} \rightarrow \mathbf{R}^+$ that encodes the extrinsic geometry of the goal is used to define the dynamics governing the associated state variables:

$$\begin{aligned} \dot{b_1} &= -D_{b_1}\left(\hat{\varphi}(s)\right) \\ \dot{\kappa} &= -D_{\kappa}\left(\hat{\varphi}(s)\right) \end{aligned}$$

3.2.4.1. Attaining Intrinsic Goal Geometry. In attaining intrinsic geometry, each robot i acts as an individual player which contributes to the generation of control input of all the torsion angles associated with K_i. The feedback-based control law that is based on artificial potential function $\check{\varphi}_i$ whose construction follows a methodology previously presented in [33]:

$$\check{\varphi}_i(s_i, w_i) = \sigma_d \circ \sigma \circ \widehat{\varphi}_i(s_i, w_i) \tag{3.11}$$

The function $\widehat{\varphi}_i : H_i \times G_i \rightarrow [0, \infty)$ uses two functions $\gamma_i : G_i \rightarrow [0, \infty)$ and $\beta_i : H_i \rightarrow [0, \infty)$ in order to encode the goal structure and the obstacles of the robots:

$$\widehat{\varphi}_i(s_i, w_i) = \frac{1000{\gamma_i}^k(w_i)}{\beta_i(s_i)} \quad k_i \in \mathbf{Z}^+ \tag{3.12}$$

While the distance from goal is encoded by the numerator $\gamma_i(w_i) = (w_i - w_{g_i})^T(w_i - w_{g_i})$ in terms of torsion angles, the denominator encodes the distance from freespace boundary by using Cartesian coordinates and is defined as $\beta_i(s_i) = \prod_{(m,j)\in Z_i} \beta_{mj}(s_i)$, where $\forall(m, j) \in Z_i, \beta_{mj}(s_i) = \delta_{mj}^2 - \rho_{mj}^2$. The freespace boundary ∂H_i is the zero level set of ${\beta_i}^{-1}(0)$ and entails robot touching each other.

Following the same procedure in the independent case, the intrinsic potential made to follow the suggestions.In other words, by using compositions intrinsic potential function can be made admissible and has a non-degenerate critical point at the goal.

3.2.4.2. Extrinsic Goal Geometry. The extrinsic geometry is attained via applying an identical control law for all the robots. This is constructed based on a simple attractive potential. The extrinsic potential function $\hat{\varphi}$ is defined as follows:

$$\hat{\varphi}(s) = (b_1 - g_1)^T(b_1 - g_1) + (\kappa - \kappa_g)^T(\kappa - \kappa_g) \tag{3.13}$$

3.2.5. Algorithm

1. Given goal s_g, compute the corresponding goal Cartesian coordinates $g_i(s_g)$,$\forall i \in P$
2. Given instant s, find the corresponding instant Cartesian coordinates $b_i(s)$,$\forall i \in P$
3. For each robot $i \in P$
   - Determine K_i – the set of robots from which it can get state data
   - Compute the control laws $-D_{\theta_i}\check{\varphi}_j(s_j)$ and $-D_{\phi_i}\check{\varphi}_j(s_j)$
4. Update θ_i and ϕ_i using the control laws $-\sum_{j=0}^{k-1} D_{\theta_i}\check{\varphi}_j(s_j)$, $-\sum_{j=0}^{k-1} D_{\phi_i}\check{\varphi}_j(s_j)$

respectively

5. Calculate the control laws $-D_{b_1}\hat{\varphi}$ and $-D_{\kappa}\hat{\varphi}$
6. Update all the robots positions by applying these control laws
7. If Termination condition is not satisfied, go to step 2 else stop

3.3. Simulation Results

In this work, for simulation purposes, we again use a Java 3D based simulator. We consider fifteen robots (31 degrees of freedom) case for simulations. The difficulty of the job is measured by the measure called tightness that is defined in Equation 2.7 in independent scenario. However, in this case the tightness is scaled by 0.1 for obtaining convenient values.

In order to measure the performance of the planner, we define a new performance measure called normalized angle length *nal*. The definition of *nal* is as follows:

$$nal = \frac{\sum_{i \in X} \int_0^{t_f} \dot{\theta}_i(t)dt + \sum_{i \in Y} \int_0^{t_f} \dot{\phi}_i(t)dt}{\sum_{i \in X} \parallel \theta_i(0) - \theta_i(t_f) \parallel + \sum_{i \in Y} \parallel \phi_i(0) - \phi_i(t_f) \parallel} \tag{3.14}$$

A small *nal* value indicates an efficiently finished job. In order to investigate the performance of the planner against Gaussian noise, the *nrc* defined in Equation 2.10 in independent scenario is used. Application of the noisy sensory case accomplished via subjecting all state readings to Gaussian noise with zero mean and given variance. If we denote the noise as η, the noisy structure information can be expressed as follows:

$$\tilde{\theta}_i = \theta_i + \eta\tilde{\phi}_i = \phi_i + \eta \tag{3.15}$$

Since as the noise level increases the collisions among robots becomes possible with a fixed step size, we expect a positive relationship between *nrc* and noise level.

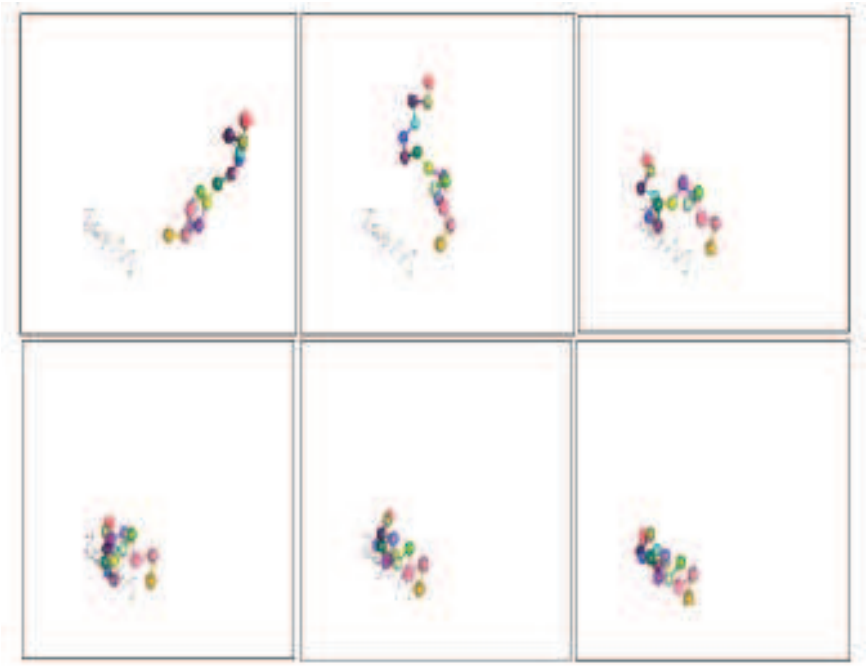

Figure 3.2. Snapshots from a simulation run of order constrained navigation

3.3.1. Complete & Perfect Sensory Case

In the first set of simulations, we use four different goal configuration with tightness values ranging from loose to packed. The goal configurations and the corresponding tightness values can be seen in Figure 3.3. We use 200 random initial configurations for simulations. The same initial configurations are used for all four final goal configurations for biasing. The results obtained can be seen from Figure 3.4. As can be seen, the tighter the goal configurations the straighter the robotic paths in terms of angles. There is an exception in the graph. The loosest goal configuration has a lower *nal* value than expected. This is because it is easy to unfold than fold. And the initial configurations are probably tighter than the loosest goal configuration. The small bars on the plot shows the standard deviation values obtained from 200 runs.

3.3.2. Complete & Noisy Sensory Case

In the second set of simulations, we try to measure the robustness of the planner to Gaussian noise. Five different levels of Gaussian noise is applied to the angle readings. The variances of the noises are 0.001 (lowest), 0.0025 (low), 0.005 (medium), 0.01 (high)

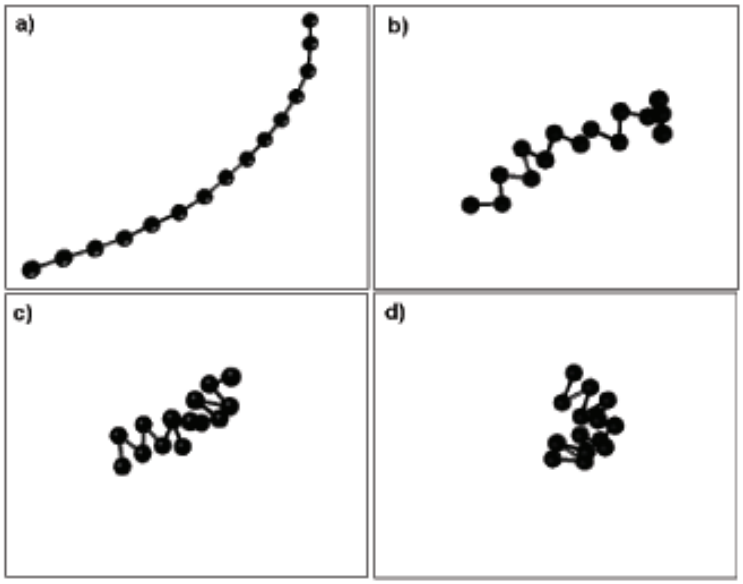

Figure 3.3. Task tightnesses of order constrained navigation. a) tight = 7.964 (relatively loose) , c) tight = 10.001, b) tight = 12.592, d) tight = 15.077 (very pack)

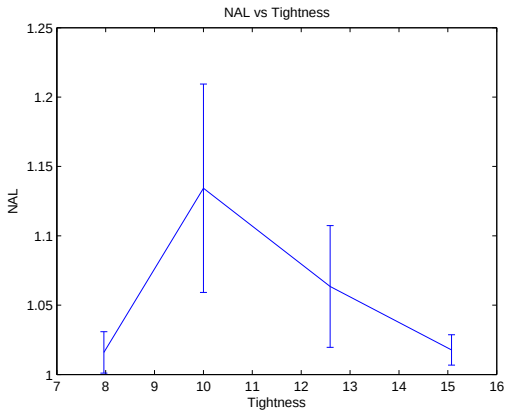

Figure 3.4. nal vs tightness of complete and perfect sensory case in order constrained navigation.

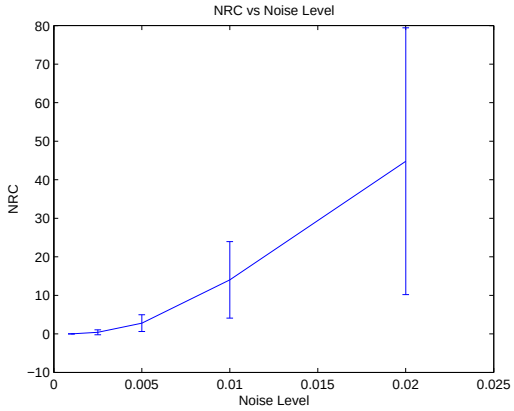

Figure 3.5. nrc vs noise level of complete and noisy sensory case in order constrained navigation.

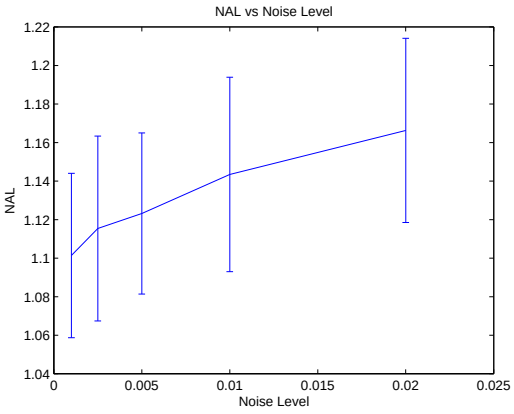

Figure 3.6. nal vs noise level of complete and noisy sensory case in order constrained navigation.

and 0.02 (highest). The tightness value of 10.001 with complete information is used for simulations. The results obtained by 200 initial configurations are shown in Figure 3.5. As expected, the noise level and the *nrc* have a positive correlation. The higher the inaccuracy, the more probable the collision among the robots. The *nal* values versus noise level is shown in Figure 3.6. It is seen that in noisy environments the robots are misguided. And as the noise level increases the probability of misguidance increases proportionally. Again in both Figure 3.5 and Figure 3.6 the small bars indicate the standard deviation values of 200 runs.

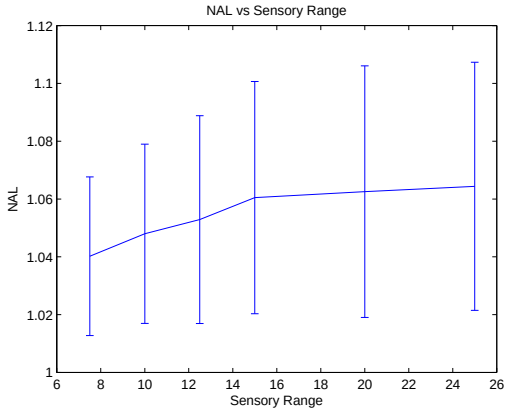

Figure 3.7. nal vs sensory range of partial and perfect sensory case in order constrained navigation.

3.3.3. Partial & Perfect Sensory Case

In the third set of simulations, the performance of the planner with partial information is investigated. The tightness value of 10.001 and noise free information is assumed. For this case, each robot is assumed to have an identical sensory range in three directions $\mu_i = [n\rho_i, n\rho_i, n\rho_i]^T$. In these simulations, $n \in \{7.5, 10, 12.5, 15, 20\}$.The result obtained from 200 initial configurations are shown in Figure 3.7. As can be seen, as the sensory range increases the *nal* value also increases. The small bars on the plot indicate the standard deviation values.

4. Application of Order Constrained Navigation to Protein Folding

4.1. Introduction

This chapter is concerned with the application of our order constrained navigation approach to protein folding kinetics with considering complete and perfect information.

Proteins are the basic building blocks of all living things. Proteins consist of amino acids and each protein has an unique order of these amino acids [52]. This order determines the type of the protein and differs it from others. With the satisfied physical conditions and with the proper amino acid sequence, a protein will automatically fold to a closely packed structure known as native structure [53]. It is believed that this native structure corresponds to the minimum free energy.

Conformational change as embodied in many biomolecular systems is one of the fundamental mechanisms. Proteins go through large structural transformations that are related to folding events and are essential for the system. Understanding the protein folding pathways is believed to reveal the nature of folding [58], [59], which will probably be a milestone for understanding the causes of various diseases associated with misfolding [60]. Experimentally determined structures of different conformers have become available over the last several years through experimental studies involving X-ray crystallography, nuclear magnetic resonance spectroscopy, cryo-electron microscopy. However, despite recent advances in these techniques, elucidating these mechanisms through direct experimental studies still remain to be difficult. Furthermore, there is no consensus as regards to whether a full mechanistic description can be obtained through experimentation alone. From this perspective, theoretical and computational models of conformational transformations have become essential if we are to develop a complete understanding of the underlying mechanisms.

4.2. Related Literature

4.2.1. Computational Biology

The studies in protein folding can be divided into two main groups: i) Structure prediction from the known amino acid sequence ([54], [55],[56], [61]) and ii) Studying protein folding kinetics to the known native structure ([57]). In this work, we assume that we know the native fold and give our attention to the protein folding kinematics.

There are different methods for protein folding kinematics investigation. The most prominent of these are Molecular dynamics simulations [62], [63], [64], [65], Monte Carlo methods [68], [69], lattice models [75], statistical mechanical models [66] , [67] and PRMs(Probabilistic Road Maps) [70], [71],[72],[73],[74].

In molecular dynamics simulation and Monte Carlo methods, the complicated true dynamics of the protein is tried to be simulated. While the path obtained from these methods are extremely reliable, they are computationally very expensive. Statistical models approximate the true dynamics by simpler molecular interactions. For example, in plastic network models, the conformational change pathways between the open and closed conformers are connected at their lowest common energies. The results are used to evaluate and analyze the minimal energy pathways between the two conformations. The open to closed transition analysis provides an identification of the hinges. Lattice models have strong theoretical ground, they cannot be applied to investigate real proteins.

4.2.2. Robotic Motion Planning Applied to Protein Folding

Recently, the robotic path planing approaches started to be applied to protein folding problem. Each conformation of a given protein can be thought as a point in the configuration space. From this point of view, proteins become the new subject of path planning approaches. These approaches, due to their relatively simpler nature, can be used to study the secondary and the tertiary structure formation order for

proteins where this has not yet been determined experimentally. In [70], a PRM based approach that was originally developed for motion planning in the robotics community is presented. Using a starting configuration and a final fold, it is able to automatically produce folding sequences for paper-folding models.

While PRM models can be valuable for investigation of folding pathways from different start conformations, their path quality is sampling dependent. Moreover, as dimension of configuration space increases the required number of samples (for protecting the same path quality) increases dramatically.

4.3. Approach

We propose to use potential fields for the investigation of protein folding kinematics. We only consider proteins whose native structures are known. Preliminary results from simulations indicate that the proposed scheme is successful in determining conformational changes. As, there is no sampling of the configuration space as is required by previous methods, it could prove to be a valuable tool for studying protein structure formation for proteins whose native structures are known.

4.3.1. Relation between Protein and Constrained Robot Structure

In order to use artificial potential fields for investigating protein folding kinetics, we construct a relationship between protein structure and a multi robot structure. In this relation the C_α atoms of proteins are represented by spherical robots. In order to represent the protein structure by these spherical robots, sequential robots are forced to stay in fixed distance throughout their motion. The configuration space of the robots is composed of the well defined torsion angles that are used in defining the protein structure in 3-D. In this representation, since the base coordinate is defined by using the structure itself, the structure's motion is independent from the space it is located. In order to define a protein structure with r number of residues, $(r-2)$ θ and $(r-3)$ ϕ angles with total of $2r-5$ angles are needed. The configuration space of the protein

structure with r residues can be defined as follows:

$$C = \{q | q \in \mathbf{SO(2r - 5)}\} \tag{4.1}$$

4.3.2. Protein Structure Parameters

Using this model, the structure of a protein can be expressed as a sequence of θ_i and ϕ_i angle pairs. These angles are calculated via the following steps

1. First extract a proteins native structure from the protein data bank (PDB), which provides coordinates for all the constituting amino acids in the native state,
2. From these coordinates, determine the bond lengths and bond angles,

The native states ϕ_i and θ_i angles can be obtained in the same way. Hence, it is possible to generate realistic configurations where the the native state structure is identical to that in PDB.

In order to compute the angles, we first let $v_i \in R^3$ to define the vector between two consecutive amino acid pair.

$$v_i = b_i - b_{i-1} \tag{4.2}$$

where b_i is the Cartesian coordinate vector of the i^{th} robot. The θ_i angle for the linked structure is defined by the following equation,

$$\theta_i = \pi - \arccos(v_i.v_{i+1}) \tag{4.3}$$

The ϕ_i angle definition is as follows:

$$\phi_i = \begin{cases} \cos^{-1}((v_{i-1} \times v_i)^T (v_i \times v_{i+1})) & \text{if} \quad v_i^T((v_{i-1} \times v_i) \times (v_i \times v_{i+1})) > 0 \\ 2\pi - \arccos((v_{i-1} \times v_i).(v_i \times v_{i+1})) & \text{else} \quad v_i^T((v_{i-1} \times v_i) \times (v_i \times v_{i+1})) \leq 0 \end{cases} \tag{4.4}$$

4.4. Simulation Results

This section presents a series of simulation studies using real protein data from the Protein Data Bank [78]. The simulations are done using a Java based simulation program designed and developed as explained earlier on. In addition to showing the temporal progression of the 3D protein folding from the initial configuration to the native configuration, the program is also capable of showing the temporal progression of the associated contact map.

In order for our approach to be useful, the results must be validated with known results. In particular, as it provides a temporal ordering of contact formations, one such validation is based on studying transition states – in particular on the comparison of formation order of the secondary and the tertiary structures [71].

The formation order is studied via recording the time of first-time occurrence of the natural contacts between C_α atoms in terms of time steps. In particular, when two C_α atoms are nearer than $7\mathring{A}$, the contacts are assumed to be formed. In order to analyze the secondary and the tertiary structure formation order, these time steps are averaged over the corresponding regions. By means of this formal approach, more detailed analysis of folding pathways can be made.

4.4.1. Sample Cases: Proteins A & GB1

We first present detailed results for two relatively small proteins: Protein A and Protein G. These proteins are selected due to two factors: i) Hydrogen exchange experimental data is available which means computational results can be compared to

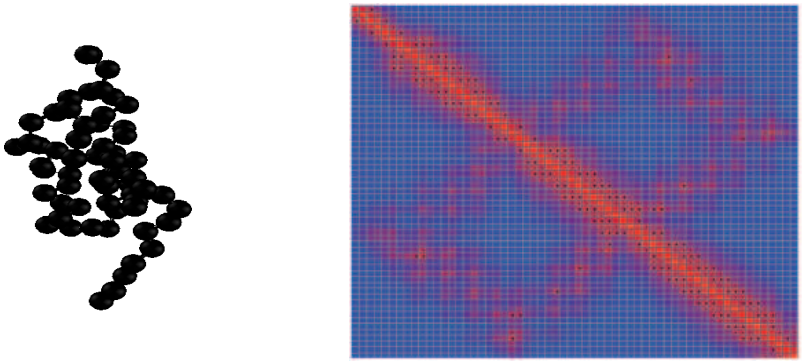

Figure 4.1. Protein A structure (60 residues) and its contact map.

those from experiments; ii) They have been studied in the previously proposed motion-planning based approaches. The PDB files used for the proteins were 1 BDD.pdb (Protein A) and 1 GB1.pdb (Protein G). respectively, from the PDB [78]. The initial conformations are taken to be the extended chain configuration. It should be remarked that the initial conformation can be selected to be any "'physically feasible"' conformation.

4.4.2. Folding of Protein A

Protein A (Staphylococcus Aureus Protein A, immunoglobulin-binding B domain) is relatively small structure with 60 residues and three α helices as seen in Figure 4.1(left). In terms of torsion angles, 60 residues corresponds to 115 degrees of freedom. The contact map of its native conformation is shown in Figure 4.1(right).

Sample snapshots of a folding trajectory is shown in Figure 4.2. In Figure 4.3 the time evolutions of the γ(attractive part of APF), β(repulsive part of APF), $\breve{\varphi}$(APF) and k parameter in the Protein A simulations are shown. As can be seen, the functions γ and β have a decreasing trend. The high jump in $\breve{\varphi}$ is resulted from increase in k value.

Figure 4.4 shows the time evolution of contacts. The blue color corresponds to no natural contact situation. As natural contacts are formed in the corresponding region, color started to turn red. Full red color represents that all the natural contacts are

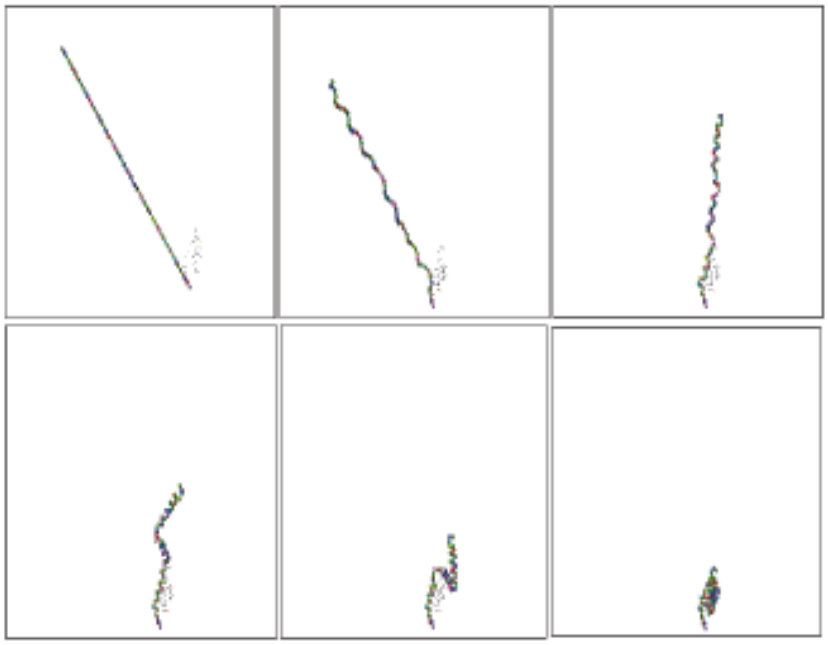

Figure 4.2. Snapshots from protein A Simulation (folding from extended conformation)

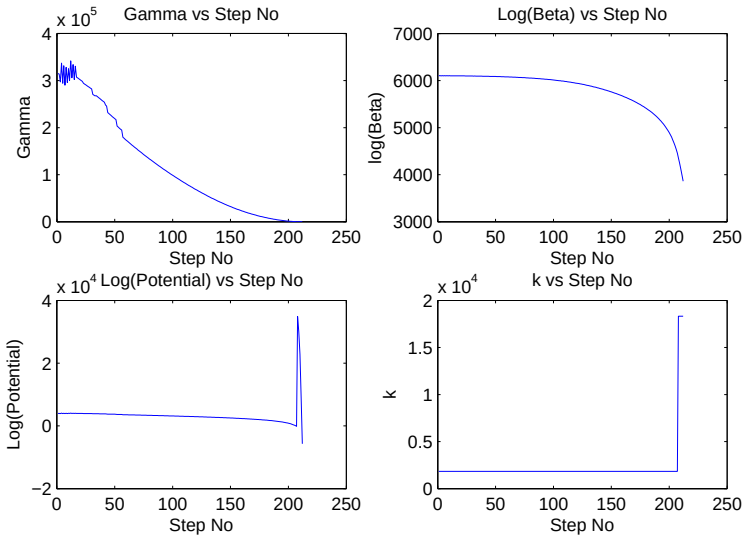

Figure 4.3. Time evolution of the γ,β, $\check{\varphi}$ and k functions in folding of protein A

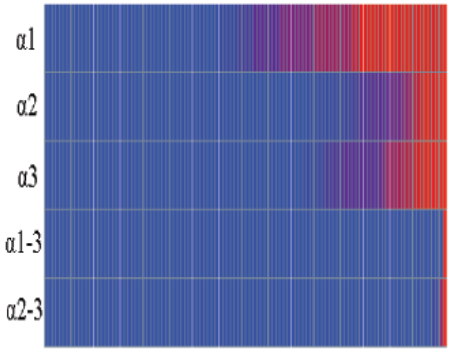

Figure 4.4. The time evolution of contacts in protein A from extended conformation.

Table 4.1. Secondary and tertiary structure formation order of protein A obtained by starting from extended conformation

Names (Regions)	α 1 (9-18)	α 2 (24-38)	α 3 (41-57)
α 1 (9-18)	177.6	N/A	212
α 2 24-38)	N/A	183.2	211
α 3 (41-57)	212	211	175.7

formed in the corresponding region. The results presented in Table 4.1 are the average times of the first time formation natural contacts among the secondary structures as explained in Section 4.4. It is observed that $\alpha 3$ helix is formed first, followed by $\alpha 1$ helix and $\alpha 2$ helix. Once the formation of the secondary structures is completed, the tertiary structures are formed. Firstly, the tertiary structure between $\alpha 2$ helix and $\alpha 3$ helix is formed. Then, the tertiary structure between $\alpha 1$ helix and $\alpha 3$ helix is formed. However, their formation times are very close to each other. Let it be noted that these results are in agreement with the experimental results as presented in [77].

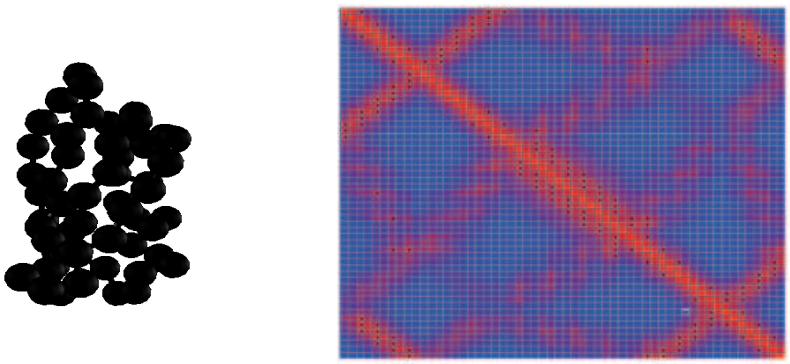

Figure 4.5. Protein G structure (56 residues) and its contact map

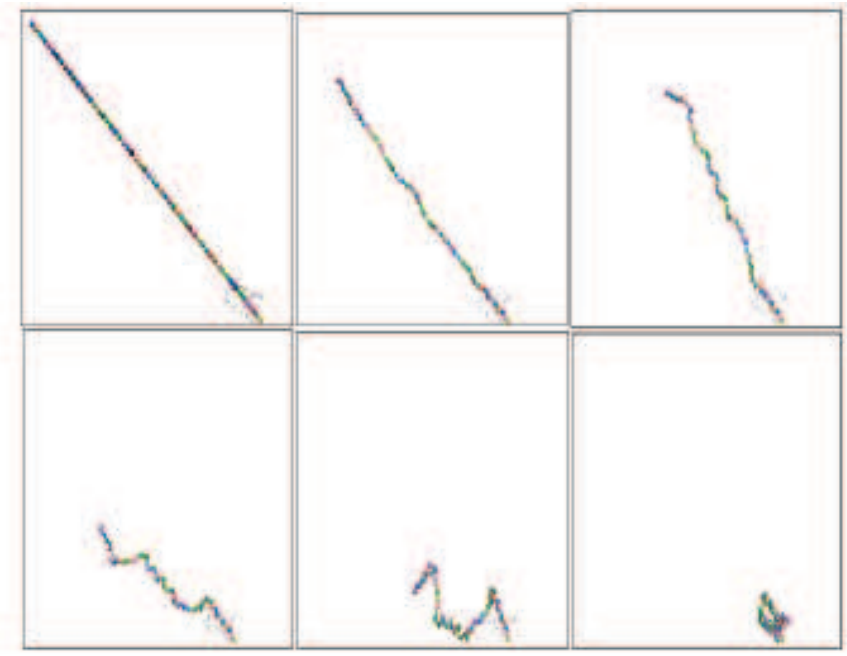

Figure 4.6. Sample snapshots from protein G Simulation (folding from extended conformation)

4.4.3. Folding of Protein G

Next, we study Protein G (streptococcal protein G, immunoglobulin-binding domain B1) as second structure which has 56 residues (107 degrees of freedom) and one α helix and four β strands as seen in Figure 4.5(left). The contact map of its native conformation is as shown Figure 4.5(right).

Sample snapshots of folding trajectory is shown in Figure 4.6. The time evolutions of the γ, β, $\breve{\varphi}$ and k parameter in protein G simulation are shown in Figure 4.7. It is observed that γ(with some little ripples) and β have a monotonically decreasing trend. The same is almost true for $\breve{\varphi}$ except for the times where the sharp increase in k value leads to a jump. The time evolution of contacts for protein G are shown in Figure 4.8.

The resulting formation order is as presented in Table 4.2. It is observed that the $\beta 1$ strand forms first. In regards to secondary and tertiary structures, experimental results [77] indicate that the α helix forms first and the tertiary structure between $\beta 1$ strand and $\beta 4$ strand forms last. This is consistent with the formation order ob-

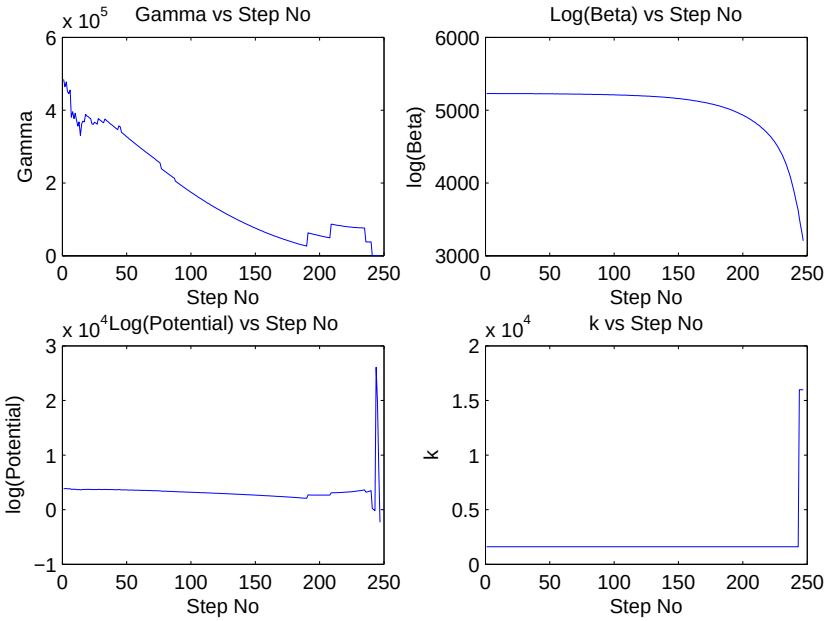

Figure 4.7. Time evolution of the γ,β, $\breve{\varphi}$ and k functions in folding of protein G

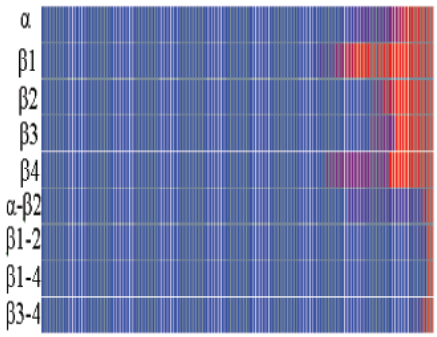

Figure 4.8. Time evolution of contacts in protein G from extended conformation

Table 4.2. Secondary and tertiary structure formation order of protein G obtained by starting from extended conformation (with time steps as units).

Names (Regions)	α (22-36)	β 1 (1-9)	β 2 (12-20)	β 3 (42-46)	β 4 (51-56)
α (22-36)	218.4	N/A	228	N/A	N/A
β 1 (1-9)	N/A	188.4	242.1	N/A	245.5
β 2 (12-20)	228	242.1	216.75	N/A	N/A
β 3 (42-46)	N/A	N/A	N/A	219	242.4
β 4 (51-56)	N/A	245.5	N/A	242.4	203

served in the simulations.

4.4.4. Statistical Studies

This section presents a series of statistical studies for the two proteins. For each protein, approximately 250 random initial conformations are generated. The generation of random configurations is realized as follows:

- The set of all transient configuration from an extended initial configuration to the native configuration as generated in Section 4.4.1 are considered,
- The set of intermediate configurations generated in the first 40% of the run are taken,
- The perturbation of total magnitude 20ϕ radians is taken,
- The number of angles to be perturbed is randomly selected to be between 1 and $2p - 5$ as denoted by N_P,
- N_P angles from all the degrees of freedom are randomly selected where each is assigned a random weight,
- Each selected angle is subjected to a perturbation where the perturbation amount is based on the ratio of its associated random weight with respect to the sum of all weights and the total perturbation magnitude,
- If the generated configuration is not physically feasible, it is discarded.

Table 4.3. The percentages of sequences in statistical runs of protein A with 239 random initial configurations

Sequence	Percentage
$\alpha 1$, $\alpha 3$, $\alpha 2$, $\alpha 2$-$\alpha 3$, $\alpha 1$-$\alpha 3$	60
$\alpha 3$, $\alpha 1$, $\alpha 2$, $\alpha 2$-$\alpha 3$, $\alpha 1$-$\alpha 3$	40

In order to analyze the variation of the generated random configurations, we study their histogram as a function of γ. Figure 4.4.4 shows this histogram for Protein A. A similar histogram of the initial configurations of Protein G is provided in Figure 4.4.4. It is observed that each set of initial configurations is away from the native configuration with approximately mean value of 3×10^5.

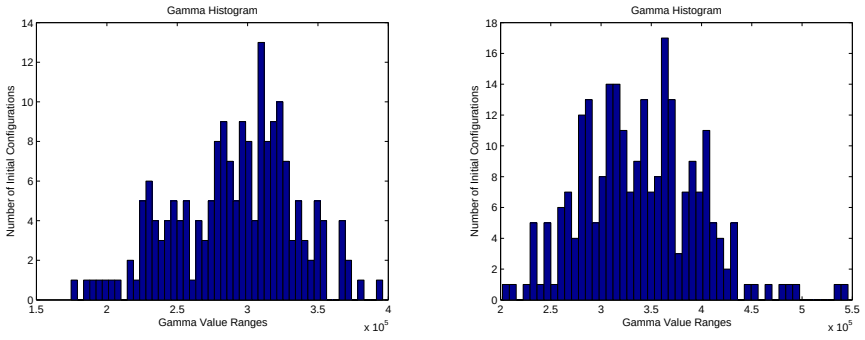

Figure 4.9. The histogram of the initial configurations as a function of γ in the simulations (protein A (left) , protein G (right))

As presented in Table 4.3, for protein A, the formation order is quite robust with two competing sequences. However, let it be noted that the two are identical except the first forming secondary structure. It is observed that while in 60% of the simulations α 1 forms first, in the remaining α 3 is the first forming secondary structure. Table 4.4 presents results for protein G.

4.4.5. Comparative Study

This section presents a comparative study of the results of our approach with a previously proposed method based on probabilistic road maps. Their agreement with the experimental data is also considered – if such data is available. For this purpose,

Table 4.4. The percentages of sequences in statistical runs of protein G with 248 random initial configurations

Sequence	Percentage
$\beta1$,$\beta4$, α ,$\beta3$,$\beta2$, α-$\beta2$, $\beta3$-$\beta4$, $\beta1$-$\beta2$, $\beta1$-$\beta4$	65
$\beta1$,$\beta4$, α ,$\beta2$,$\beta3$, α-$\beta2$, $\beta3$-$\beta4$, $\beta1$-$\beta2$, $\beta1$-$\beta4$	22
$\beta1$,$\beta4$, $\beta2$, α, $\beta3$, α-$\beta2$, $\beta3$-$\beta4$, $\beta1$-$\beta2$, $\beta1$-$\beta4$	11
$\beta1$,$\beta4$, $\beta2$, $\beta3$, α, α-$\beta2$, $\beta3$-$\beta4$, $\beta1$-$\beta2$, $\beta1$-$\beta4$	2

Table 4.5. Comparison of our method with [73] and experimental results presented in [77]

PDB Code	p (#DOF)	APF-Based Method	PRM-Based Method [73]	Exp. [77]
1GB1	56 (107)	$\alpha1$, $\beta3$-$\beta4$, $\beta1$-$\beta2$, $\beta1$-$\beta4$	$\alpha1$, $\beta3$-$\beta4$, $\beta1$-$\beta2$, $\beta1$-$\beta4$	Agreed
1BDD	60 (115)	$\alpha1$, $\alpha3$, $\alpha2$, $\alpha2$-$\alpha3$, $\alpha1$-$\alpha3$	$\alpha2$, $\alpha3$, $\alpha1$, $\alpha2$-$\alpha3$, $\alpha1$-$\alpha3$	Agreed
1SRL	56 (107)	$\beta4$-$\beta5$, $\beta3$-$\beta4$, $\beta2$-$\beta3$, $\beta1$-$\beta5$, $\beta1$-$\beta2$	$\beta4$-$\beta5$, $\beta3$-$\beta4$, $\beta2$-$\beta3$, $\beta1$-$\beta5$,$\beta1$-$\beta2$	N/A
1NYF	58 (111)	$\beta3$-$\beta4$, $\beta2$-$\beta3$, $\beta1$-$\beta2$	$\beta3$-$\beta4$, $\beta2$-$\beta3$, $\beta1$-$\beta2$	N/A
1SHG	57 (109)	$\beta3$-$\beta4$,$\beta2$-$\beta3$,$\beta1$-$\beta5$,$\beta1$-$\beta2$	($\beta2$-$\beta3$ $\beta3$-$\beta4$), ($\beta1$-$\beta2$ $\beta1$-$\beta5$)	N/A
1UBQ	78 (147)	$\alpha1$, $\beta3$-$\beta4$, $\beta1$-$\beta2$, $\beta3$-$\beta5$, $\beta1$-$\beta5$	$\alpha1$, $\beta3$-$\beta4$, $\beta1$-$\beta2$, $\beta3$-$\beta5$, $\beta1$-$\beta5$	Agreed

we simulate 6 different protein structures, and compare the order of secondary and tertiary structure occurrence with the order obtained by search based method in [73]. Table 4.5 shows the secondary and tertiary structure formation order obtained by both methods and those based on experimental data – if available. Note that the first two proteins correspond to Protein G and Protein A respectively. In general, the formation order of the secondary and the tertiary structures on our paths agrees with known computational and experimental results. Our preliminary findings show that this approach is a potentially valuable tool since in contrast to planning based approaches, its computational complexity does not grow exponentially with the size of the proteins.

5. CONCLUSIONS

This thesis investigates the coordinated navigation of multi-robot teams. Two different scenarios are considered – independent and order constrained navigation. In independent navigation, robots can move independently and simultaneously with each other. In order constrained navigation, the robots are assumed to have an sequential order and an imaginary link with a fixed distance constraint is assumed to exist between any two consecutive robots. In both scenarios, each robot may have a sensory range varying from infinite to myopic that determine which other robots it can communicate and hence get information from. Our approach is based on artificial potential functions. In each scenario, a family of of artificial potential function that embed both the goal and the dynamic obstacles known to each robot is constructed. In the independent case, the motion of each robot is then realized through first-order dynamics where the control law is constructed based on the negative gradient of this artificial potential function. In the order constrained case, the motion of each robot is governed through a control law that is constructed based on two tiers. The first tier governs the motion of each robot towards attaining the overall intrinsic geometry while the second level moves the aggregate system towards the overall extrinsic geometry. Each scenario is studied through extensive simulations with varying difficulty of tasks and noise levels. Order constrained navigation is then applied to study protein folding kinematics. It is shown that the results obtained from our simulations are consistent with the known experimental results. In summary, our preliminary results indicate that our approach based on artificial potential functions to be promising in studying both robotic formations and protein folding. As part of our ongoing research, we are working on the theoretical analysis of both cases.

APPENDIX A: Adjusting k parameter of APF in Protein Folding Simulation

1. Given goal s_g, instant s states and the corresponding instant Cartesian coordinates $b_i(s)$
2. Take a robot i from robot set P
3. Compute the APF $\breve{\varphi}_i$(Since complete and perfect information case is considered for protein folding kinetics, all robots have the same APF)
4. If APF ¡ 1 and γ_i ¿ 1
   - while APF ¡ 1
     . $k = k * 2$

REFERENCES

1. Chirikjian, G. S., *Theory and Applications of Hyper-Redundant Robotic Manipulators*, Ph.D Dissertation, Department of Applied Mechanics, Division of Engineering and Applied Science, California Institute of Technology, June, 1992.

2. Chirikjian, G. S., and J. W. Burdick, "An Obstacle Avoidance Algorithm for Hyper-Redundant Manipulators", *Proc. of IEEE ICRA90*, Cincinnati, OH, May, 1990.

3. Hirose, S., *Biologically Inspired Robots, Snake-Like Locomotors and Manipulators*, Oxford University Press, Oxford, 1993.

4. Chirikjian, G. S., "Kinematic synthesis of mechanisms and robotic manipulators with binary actuators", *ASME J. Mech. Des. 117*, no. 4, pp. 573-580, 1995.

5. Hannan, M. W., and I. D. Walker, "The Elephant Trunk Manipulator, Design and Implementation", *Proc. of the 2001 IEEE/ASME AIM*, Italy, 2001.

6. Yim, M., "A Reconfigurable Modular Robot with Manu Modes of Locomotion", *Proc. of 1993 JSME Intl Conf. on Adv. Mechaton*, Japan, 1993.

7. Hickman, F., W. Henning, and H. Choset, "Motion Planning for Serpentine Robots", *ASCE Space and Robotics*, USA, 1998.

8. Lozano-Perez, T., "Spatial planning: A configuration space approach", *IEEE Transactions on Computers*, vol. C-32, pp. 108-120, IEEE Press, 1983.

9. Kavraki, L., P. Svestka, J. C. Latombe, and M. Overmars, "Probabilistic roadmaps for path planning in high-dimensional configuration spaces", *IEEE Trans. Robot. Automat.*, pp. 12(4):566-580, 1996.

10. Kuffner, J. and S. LaValle, "RRT-connect: An efficient approach to single-query path planning", *Proceedings of the IEEE Intnational Conference on Robotics and*

Automation (ICRA), April 2000.

11. Nakagaki, H. and K. Kitagaki, "Study of deformation tasks of a flexible wire", *Proc. of IEEE Int. Conf. on Robotics and Automation*, 1997.

12. Gayle, R., P. Segars, M. Lin, and D. Manocha, "Path planning for deformable robots in complex environments", University of North Carolina-Chapel Hill, Tech. Rep., *Proc. of Robotics: Science and Systems*, 2005.

13. Ladd, A. and L. Kavraki, "Using motion planning for knot untangling", *International Journal of Robotics Research*, vol. 23, no. 7-8, pp. 797-808, 2004.

14. Pisula, C., K. Hoff, M. Lin and D. Manocha, "Randomized path planning for a rigid body based on hardware accelerated voronoi sampling", *Proc. of 4th International Workshop on Algorithmic Foundations of Robotics*, 2000.

15. Guibas, L., C. Holleman, and L. Kavraki, "A probabilistic roadmap planner for flexible objects with a workspace medial-axis-based sampling approach", *Proc. of IROS*, 1999.

16. Wilmarth, S., *A probabilistic method for rigid body motion planning using sampling from the medial axis of the free space*, Ph.D. dissertation, Texas A &M University, Dec 1999.

17. Amato, N., O. Bayazit, L. Dale, C. Jones, and D. Vallejo, "OBPRM: An obstacle-based PRM for 3D workspaces", *Proceedings of WAFR98*, pp. 197-204, 1998.

18. Burns, B. and O. Brock, "Toward optimal configuration space sampling", *Proceedings of Robotics: Science and Systems*, 2005.

19. Yershova, A., L. Jaillet, T. Simeon, and S. M. LaValle, "Dynamicdomain RRTs: Efficient exploration by controlling the sampling domain", *Proceedings IEEE International Conference on Robotics and Automation*, 2005.

20. Koditschek, D. E., "Exact robot navigation by means of potential functions: some topological considerations", *Proc. IEEE Int. Con. Robot. Automat.*, Raleigh, NC, pp. 1-6, 1987.

21. Barraquand, J. and J. C. Latombe, "Robot motion planning: a distributed representation approach", *Inc. J. Robot. Res.*, vol. 10, pp. 628-649, 1991.

22. Rimon, E. and D. E. Koditschek, "Exact robot navigation using artificial potential functions", *IEEE Trans. Robot. Automat.*, vol. 8, pp. 501-518, 1992.

23. Faverjon, B. and P. Tournassoud, "A local approach for path planning of manipulators with a high number of degrees of freedom", *Proc. IEEE Int. Con. Robotics andAutomation*, Raleigh, NC, pp. 1152-1159, 1987.

24. Faverjon, B. and P. Tournassoud, "A practical approach to motion planning for manipulators with many degrees of freedom", *Robotics Research 5*, H. Minra and S. Arimoto, Eds. Cambridge, MA: MIT Press, p. 65-73, 1990.

25. Barraquand, J., B. Langlois and J. C. Latombe, "Numerical potential field techniques for robot path planning", *IEEE Trans. Syst. Man. Cybern.*, vol. 22, no. 2, pp. 224-241, 1992.

26. Graux, L., P. Millies, P. L. Kociemba, and B. Langlois, "Integration of a path generation algorithm into off-line programming of airbus panels", *Aerospace Automated Fastening Con. and Exp.*, SAE Tech. Paper 922404, Oct. 1992.

27. Koga, Y., K. Kondo, J. Kuffner, and J. C. Latombe, "Planning motions with intentions", *Proc. SIGGRAPH94*, pp. 395-408, 1994.

28. Chanclou, B. and A. Luciani,"Global and local path planning in natural environment by physical modeling", *Intelligent Robots and Systems '96, IROS 96. Proceedings of the 1996 IEEERSJ International Conference on Volume: 3*, vol. 3, pp. 1118-1125, 1996.

29. Plumer, E. S., "Neural network structure for navigation using potential fields", *Proc. Int. Joint Conf. Neural Networks (IJC-92)*, vol. 1, pp. 327-332, 1992.

30. Akishita, S., T. Hisanobu and S. Kawamura, "Fast path planning available for moving obstacle avoidance by use of Laplace potential", *Intelligent Robots and Systems '93, IROS '93. Proceedings of the 1993 IEIEE/RSJ International Conference on Volume: 1*, vol. 1, pp. 673-678, 1993.

31. Makita, Y., M. Hagiwara and M. Nakagawa, "A simple path planning system using fuzzy rules and a potential field", *Fuzzy Systems, 1994 IEEE World Congress on Computational Intelligence, Proceedings of the Third IEEE Conference on Volume 2*, vol. 2, pp. 994 -999, 1994.

32. Wu, K. H., C. H. Chen and J. D. Lee, "Genetic-based adaptive fuzzy controller for robot path planning", *Fuzzy Systems, 1996, Proceedings of the Fifth IEEE International Conference on Volume: 3*, vol. 3, pp. 1687-1692, 1996

33. Karagöz, C. S., H. I. Bozma and D. E. Koditschek, "Coordinated Navigation of Multiple Independent Disk-Shaped Robots", Technical Report, CSE-TR-486-04, The University of Michigan, Computer Science and Engineering Division, Department of Electrical Engineering and Computer Science, February 2004.

34. Karagöz, C. S. *A Game-Theoretic Approach to Objects' Moving Problem With Mobile Robots*, Ph.D. Thesis, Electric Electronic Engineering, Bogazici University, 2001.

35. Koditschek, D. E., "Task Encoding: Toward a Scientific Paradigm for Robot Planning and Control", *Robotics and Autonomous Systems*, Vol. 9, pp. 5-39, Elsevier, 1992.

36. LaValle, S. M. and S. Hutchinson, "Optimal Motion Planning for Multiple Robots Having Independent Goals", *IEEE Transactions on Robotics and Automation*, V 14, No 6, pp. 912-925, 1998.

37. Koren, Y. and J. Borenstein, "Potential Field Methods and Their Inherent Limitations for Mobile Robot Navigation", *P*roceedings of the IEEE International Conference on Robotics and Automation, pp. 1398-1404, Sacramento, California, April 1991.

38. Khatib, O., "Real Time Obstacle Avoidance for Manipulators and Mobile Robots", *International Journal of Robotics Research*, Vol. 5, No. 1, pp. 90-99, 1986.

39. Ramanathab, G. and V.S. Alagar, "Algorithmic Motion Planning in Robotics: Coordinated Motion of Several Disks Amidst Polygonal Obstacles", *P*roceedings of the IEEE International Conference on Robotics and Automation, pp. 514-522, March 1985.

40. Siméon, T., S. Leroy and J. Laumond, "Path Coordination for Multiple Mobile Robots: A Resolution-Complete Algorithm", *I*EEE Transactions on Robotics and Automation, Vol. 18, No. 1, pp. 42-49, February 2002.

41. Warren, C. "Multiple Robot Path Coordination Using Artificial Potential Functions", *P*roceedings of the IEEE International Conference on Robotics and Automation, pp. 500-505, 1990.

42. Balch, T. and R. C. Arkin, "Behavior-Based Formation Control for Multirobot Teams", *IEEE Transactions on Robotics and Automation*, V 14, pp. 926-939, 1998.

43. Ge, S. S. and Y. J. Cui, "Dynamic Motion Planning for Mobile Robots Using Potential Field Method", *Autonomous Robots*, V 13, pp. 207-222, 2002.

44. Svetska, P. and M. H Overmars, "Coordinated Motion Planning for Multiple Car-Like Robots using Probabilistic Roadmaps", *Proceedings of the IEEE Int. Conference on Robotics and Automation*, pp. 1631-1636, 1995.

45. Peng, J. and S. Akella, "Coordinating Multiple Double Integrator Robots on a Roadmap: Convexity and Global Optimality", *Proceedings* of the IEEE Int. Con-

ference on Robotics and Automation, pp. 2762-2769, 2005.

46. Ogren, P. and N. E. Leonard, "Obstacle Avoidance in Formation", *Proceedings of the 2003 IEEE Internationai Conference on Robotics and Automation*, Taipei, Taiwan, 2003.

47. Schneider, F. E. and Dennis Wildermuth, "A potential field based approach to multi robot formation navigation", *Proceedings of the 2003 IEEE International Conference on Robotics*, Intelligent Systems and Signal Processing, Changsha, China, 2003.

48. Latombe, J. C., *Robot Motion Planning*, Boston, MA: Kluwer Academic Publishers, 1991.

49. Sheng, X., "Motion planning for computer animation and virtual reality applications", *Proceedings of the Computer Animation*, p. 56, 1995

50. Kalisiak, M. and M. van de Panne, "A Grasp-based Motion Planning Algorithm for Intelligent Character Animation", *Eurographics Workshop on Computer Animation and Simulation*, 2000.

51. Chang, H. and T. Y. Li, "Assembly Maintainability Study with Motion Planning", *Proc. IEEE Int. Conf. on Robotics and Automation*, pp. 1012-1019, 1995.

52. Branden, C. and J. Tooze, *Introduction to Protein Structure (2nd edition)*, New York: Garland Pub., 1999.

53. Anfinsen, C. B., "Principles that govern the folding of protein chains", *Science*, vol. 181, pp. 223-230, 1973.

54. Reeke, G. N., "Protein folding: Computational approaches to an exponential-time problem", *Ann. Rev. Comput. Sci.*, vol. 3, pp. 59-84, 1988.

55. Levitt, M., M. Gerstein, E. Huang, S. Subbiah, and J. Tsai, "Protein folding: The

endgame", *Annu. Rev. Biochem.*, vol. 66, pp. 549-579, 1997.

56. Sun, S.,"Reduced representation model of protein structure prediction: Statistical potential and genetic algorithms", *Protein Sci.*, vol. 2, no. 5, pp. 762-785, 1993.

57. Munoz, V. and W. A. Eaton, "A simple model for calculating the kinetics of protein folding from three dimensional structures", *Proc. Natl. Acad. Sci. USA*, vol. 96, no. 20, pp. 11311-11316, 1999.

58. Honig, B., "Protein folding: From the Levinthal Paradox to structure prediction", *J. Mol. Biol.*, vol. 293, pp. 283-293, 1999.

59. Shakhnovich, E.I., Theoretical studies of protein-folding thermodynamics and kinetics, Curr. Op. Str. Biol., vol. 7, pp. 29-40, 1997.

60. Lansbury, P.T., "Evolution of amyloid: What normal protein folding may tell us about fibrillogenesis and disease", *Proc. Natl. Acad. Sci. USA*, vol. 96, no. 7, pp. 3342-3344, 1999.

61. Sternberg, M. J., *Protein Structure Prediction: A Practical Approac*h, Oxford: IRL Press at Oxford University Press, 1996.

62. Levitt, M., "Protein folding by restrained energy minimization and molecular dynamics", *J. Mol. Biol.*, vol. 170, pp. 723-764, 1983.

63. Daggett, V. and M. Levitt, "Realistic simulation of naive-protein dynamics in solution and beyond", *Annu. Rev. Biophys. Biomol. Struct.*, vol. 22, pp. 353-380, 1993.

64. Duan, Y. and P.A. Kollman, "Pathways to a protein folding intermediate observed in a 1-microsecond simulation in aqueous solution", *Science*, vol. 282, pp. 740-744, 1998.

65. Haile, J.M., *Molecular Dynamics Simulation: Elementary Methods*, New York:

Wiley, 1992.

66. Alm, E. and D. Baker, "Prediction of protein-folding mechanisms from freeenergy landscapes derived from native structures", *Proc. Natl. Acad. Sci. USA*, vol. 96, no. 20, pp. 11305-11310, 1999.

67. Baker, D., "A surprising simplicity to protein folding", *Nature*, vol. 405, pp. 39-42, 2000.

68. Covell, D.G., "Folding protein -carbon chains into compact forms by Monte Carlo methods", *Proteins: Struct. Funct. Genet.*, vol. 14, no. 4, pp. 409-420, 1992.

69. Kolinski, A. and J. Skolnick,"Monte Carlo simulations of protein folding", *Proteins Struct. Funct. Genet.*, vol. 18, no. 3, pp. 338-352, 1994.

70. Song, G. and N. M. Amato,"A motion planning approach to folding: From paper craft to protein folding", *IEEE Trans. Robot. Automat.*, 2003.

71. Amato, N. M. and G. Song, "Using motion planning to study protein folding pathways", *J. Comput. Biol.*, vol. 9, no. 2, pp. 149-168, 2002.

72. Amato, N. M., Ken A. Dill, and G. Song, "Using motion planning to map protein folding landscapes and analyze folding kinetics of known native structures", *Proc. Int. Conf. Comput. Molecular Biology (RECOMB)*, pp. 2-11, Washington DC, 2002.

73. Amato,N. M., Ken A. Dill, and G. Song, "Using motion planning to map protein folding landscapes and analyze folding kinetics of known native structures", *J. Comput. Biol.*, vol. 10, no. 3-4, pp. 239-256, 2003.

74. Song, G., S.L. Thomas, K.A. Dill, J.M. Scholtz, and N.M. Amato, "A path planning-based study of protein folding with a case study of hairpin formation in protein G and L", *Proc. Pacific Symposium of Biocomputing (PSB)*, pp. 240-251, Lihue, HI, 2003.

75. Bryngelson, J.D., J.N. Onuchic, N.D. Socci, and P.G. Wolynes, "Funnels, pathways, and the energy landscape of protein folding: A synthesis", *Protein Struct. Funct. Genet.*, vol. 21, pp. 167-195, 1995.

76. Khatib, O., "Real-time obstacle avoidance for manipulators and mobile robots", *Int. J. for Robotics Research*, Vol. 5, NO. 1, pp. 90-99, 1986.

77. Li,R. and C. Woodward, "The hydrogen exchange core and protein folding", *Protein Sci.*, vol. 8, pp. 1571-1591, 1999.

78. *The Protein Data Bank*, http://www.rcsb.org/pdb/, 2006.

REFERENCES NOT CITED

Mattice, Wayne L. and Ulrich W. Suter, *Conformational Theory of Large Molecules*, Wiley-Interscience, New York, 1994.